Visco-plasticity stress-based solid dynamics formulation and time-stepping algorithms for stiff case

Cong Uy Nguyen, Adnan Ibrahimbegovic

Version of Record: https://www.sciencedirect.com/science/article/pii/S0020768320301347
Manuscript_da60b88acbe5b1d6154c9362acec326a

Visco-plasticity stress-based solid dynamics formulation and time-stepping algorithms for stiff case

Cong Uy Nguyen[a] and Adnan Ibrahimbegovic[a,b,c] *

[a]Université de Technologie de Compiègne (UTC)/ Alliance Sorbonne Université, Laboratoire Roberval de Mécanique, Centre de Recherche Royallieu, 60200 Compiègne, France ; [b]Chaire de Mécanique UTC ; [c]Institut Universitaire de France (IUF)

Abstract

In this paper, the visco-plastic behavior of solids is formulated based on the Hellinger-Reissner variational principle. The latter provides an optimal basis to obtain an increased accuracy of computed stress by using independent space-discretizations of both displacement and stress fields. The formulation is further adapted to solid dynamics and in particular to so-called stiff case that is characterized with a large difference in stiffness and/or evolution time between different deformation modes, which presents a great challenge when integrating the dynamic response. For this class of problem, we here propose the algorithmic modifications leading to energy conserving or decaying schemes that can either preserve the total energy or dissipate the energy of higher modes, and thus control the overall stability of numerical computations with large steps over long period of time. Several numerical examples are presented to illustrate a very satisfying performance of the proposed approach and algorithm.

Keywords: Helligner-Reissner formulation, visco-plasticity, dynamic response, stiff solids, energy conserving/decaying schemes

1 Introduction

This work seeks to contribute on formulating the time integration scheme for nonlinear dynamics of stiff systems undergoing visco-plasticity phenomena. The proposed solution concerns two research fields in computational mechanics that have been receiving a great attention over the years. The classical algorithm for visco-plasticity can be found in literature, see [Zienkiewicz and Cormeau, 1974, Hughes and Taylor, 1978]. In these studies, the partial differential governing equations of visco-plasticity are discretized and solved numerically via the traditional finite element method. Only displacement is considered as independent field in the discrete approximation of the weak form of governing equations, which is then examined under static or dynamic loading conditions by using operator split method for plasticity [Ibrahimbegovic, 2009] that always lead to the first-order time integration schemes [Chorin et al., 1978]. There are several other researches relevant to visco-plasticity problem, especially in metal forming and cutting [Pipard et al., 2013, Mahnken et al., 2013].

Here, the conventional visco-plasticity problem is formulated by using the Helligner-Reissner approach and the finite element method. This approach enlarges the solution space including displacement and stress fields, which increases the stress accuracy, see [Auricchio et al., 2013, Auricchio et al., 2015]. Less computational cost can be obtained by using this method since it

*Corresponding author, Professor, E-mail: adnan.ibrahimbegovic@utc.fr

can yield an accurate solution even in a coarse mesh and especially in incompressible condition, see [Viebahn et al., 2018]. This advantage can be observed in the numerical examples with both displacement and stress fields considered as independent fields. This visco-plasticity problem is further generalized to dynamics, in which the inertia force plays role in the governing equations of a system.

In order to deal with dynamics applications of interest for this work, proper time-stepping scheme should be proposed to compute structural responses over long period of time. Here, the stability of the time integration scheme must be maintained over a large number of time steps. Several time-stepping schemes for dynamic problems are successfully developed, which are proved to remain stable for long-term computation, see [Bathe and Baig, 2005, Hilber et al., 1977, Erlicher et al., 2002]. In the visco-plasticity problem, the dissipative property of energy does not guarantee the numerical stability of time-stepping schemes, which is very important quality for numerical computation. For that reason, the energy conserving scheme is introduced so that the total energy of system, consisting of the kinetic and potential energies, is always preserved in the elastic regime unless the visco-plastic dissipation starts to evolve due to visco-plastic strain in a system when the stresses satisfy the yield criteria.

The proposed scheme can support the computation for a long period of time for several particular physic problems, providing the estimate of plastic evolution in long-time. The underlying idea of this scheme is the combination of mid-point time integration scheme and algorithmic equations for the computation of displacement and stress within an interval of time step. In the view of computational accuracy, the mid-point time integration scheme is well-known for the higher accuracy compared to other schemes such as backward or forward Euler method [Ibrahimbegovic, 2009]. For higher accuracy of stress with coarse finite element mesh, we also introduce a modified energy conserving scheme that can lead to the energy decaying scheme, since it is desirable to dissipate the contribution of higher frequencies and corresponding modes to the computed nonlinear response of a stiff system. We follow the approach [Ibrahimbegovic and Mamouri, 2002, Armero, 2006], the variation of velocities and stress computation within a time interval is modified so that it reduces the participation of high-frequency modes in controllable manner via dissipation coefficients α and β.

The paper outline is as follows. The theoretical formulation of visco-plasticity problem using Hellinger-Reissner functional is presented in the Section 2. It is noted that this study is restricted to structural behavior undergoing only small strain. Section 3 is devoted to numerical implementation of visco-plasticity problem including the discretization of the physical domain and time-dependent variables. In addition, the energy conserving and decaying schemes are formulated to control the overall energy of system and dissipate higher frequency modes. In Section 4, several selective simulations of the visco-plasticity problem in a thick-walled pipe under dynamic loading scenarios are simulated. In Section 5, our finding is finally summarized by the conclusions and discussions.

2 Theoretical formulation of visco-plasticity problem

In this section, the Hellinger-Reissner variational principle is employed for visco-plasticity at small strain. Let Ω be a bounded domain in $\mathbb{R}^3$ with piece-wise smooth boundary $\partial\Omega$, satisfying

$$\partial\Omega = \partial\Omega_1 \cup \partial\Omega_2 \quad \text{and} \quad \partial\Omega_1 \cap \partial\Omega_2 = \emptyset \tag{2.1}$$

where $\partial\Omega_1$ denotes the displacement boundary and $\partial\Omega_2$ the stress boundary.

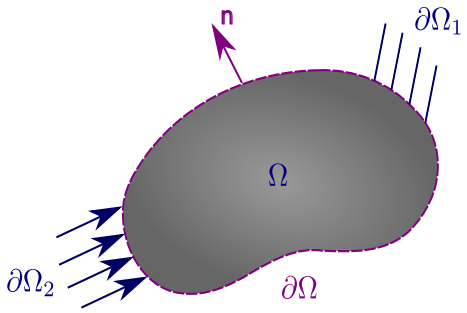

Fig. 1: The domain Ω and its boundary $\partial\Omega$ with indicated boundary conditions

The linear total strain $\boldsymbol{\epsilon}(\boldsymbol{u})$ tensor in small strain theory is defined by the symmetric gradient of displacement displacement $\boldsymbol{u}$ field as in Eq. (2.2).

$$\boldsymbol{\epsilon}(\boldsymbol{u}) := \nabla^s \boldsymbol{u} = \frac{1}{2}\left(\nabla \boldsymbol{u} + (\nabla \boldsymbol{u})^T\right) \tag{2.2}$$

The symbol $\nabla \boldsymbol{u}$ denotes the gradient of a displacement $\boldsymbol{u}$ vector, e.g. $\nabla \boldsymbol{u} = [u_{i,j}]$. The above total strain tensor is assumed as a combination of elastic strain $\boldsymbol{\epsilon}^e$ tensor and visco-plastic strain $\boldsymbol{\epsilon}^{vp}$ tensor, hence we have the relation $\boldsymbol{\epsilon}^e = \boldsymbol{\epsilon} - \boldsymbol{\epsilon}^{vp}$. The problem of visco-plasticity at small strains is characterized by the strain energy functional $\Pi^{int}(\boldsymbol{u})$ as follows:

$$\Pi^{int}(\boldsymbol{u}) = \int_\Omega \psi^e\left(\boldsymbol{\epsilon} - \boldsymbol{\epsilon}^{vp}\right) \mathrm{d}V \tag{2.3}$$

where the elastic free energy density function $\psi^e\left(\boldsymbol{\epsilon} - \boldsymbol{\epsilon}^{vp}\right)$ is a function of elastic strain tensor:

$$\psi^e\left(\boldsymbol{\epsilon} - \boldsymbol{\epsilon}^{vp}\right) = \frac{1}{2}\left(\boldsymbol{\epsilon} - \boldsymbol{\epsilon}^{vp}\right) : \mathbb{C} : \left(\boldsymbol{\epsilon} - \boldsymbol{\epsilon}^{vp}\right) \tag{2.4}$$

with $\mathbb{C}$ as the fourth-order elasticity tensor. The symbol ':' stands for the double contraction operation, e.g. $\boldsymbol{A} : \boldsymbol{B} = A_{ij}B_{ij}$ (two second order tensor) and $\mathbb{A} : \boldsymbol{B} = \mathbb{A}_{ijkl}B_{kl}$ (fourth and second order tensors). From such elastic free energy function, the relationship between stress $\boldsymbol{\sigma}$ tensor and elastic strain $\boldsymbol{\epsilon}^e$ tensor can be derived as

$$\boldsymbol{\sigma} := \frac{\partial \psi^e(\cdot)}{\partial \boldsymbol{\epsilon}} = \mathbb{C} : \left(\boldsymbol{\epsilon} - \boldsymbol{\epsilon}^{vp}\right)$$

In visco-plasticity problem, the yield function $\phi(\boldsymbol{\sigma})$ governs the evolution of visco-plastic strain $\boldsymbol{\epsilon}^{vp}$ along with time. The negative value of the yield function indicates the elastic regime without the development of visco-plastic strain ($\dot{\boldsymbol{\epsilon}}^{vp} = 0$). Any non-negative value of the yield function implies the visco-plastic regime, with the corresponding change of visco-plastic strain ($\dot{\boldsymbol{\epsilon}}^{vp} \neq 0$) according to:

$$\phi(\boldsymbol{\sigma}) := \operatorname{sgn} F\, |F|^m; \quad F = 3J_2/\sigma_y^2 - 1; \quad \begin{cases} \phi(\boldsymbol{\sigma}) \leq 0 \Rightarrow \dot{\boldsymbol{\epsilon}}^{vp} = \boldsymbol{0} \\ \phi(\boldsymbol{\sigma}) > 0 \Rightarrow \dot{\boldsymbol{\epsilon}}^{vp} \neq \boldsymbol{0} \end{cases} \tag{2.5}$$

where σ_y is the yield stress and J_2 is the stress invariant. The dot in $\dot{\boldsymbol{\epsilon}}^{vp}$ denotes the derivative of visco-plastic strain with respect to time, or the rate of visco-plastic strain. In this study, we choose the parameter value $m = 1$ in Eq. (2.5); we thus recover the classical viscoplasticity model (e.g. [Ibrahimbegovic et al., 1998]), where the corresponding yield function accepts all admissible values in $\mathbb{R}$ as follows:

$$\phi \equiv F = 3J_2/\sigma_y^2 - 1; \quad J_2 = \frac{1}{2}\operatorname{dev}(\boldsymbol{\sigma}) : \operatorname{dev}(\boldsymbol{\sigma}) \tag{2.6}$$

where the operator dev($\boldsymbol{\sigma}$) stands for the deviatoric part of stress tensor $\boldsymbol{\sigma}$. The external load potential $\Pi^{ext}(\boldsymbol{u})$ and kinetic energy $K(\dot{\boldsymbol{u}})$ are written as follows:

$$\Pi^{ext}(\boldsymbol{u}) = \int_{\Omega} \boldsymbol{f} \cdot \boldsymbol{u} \mathrm{d}V + \int_{\partial\Omega_2} \boldsymbol{t} \cdot \boldsymbol{u} \mathrm{d}A \quad ; \quad K(\dot{\boldsymbol{u}}) = \frac{1}{2} \int_{\Omega} \rho \dot{\boldsymbol{u}} \cdot \dot{\boldsymbol{u}} dV \tag{2.7}$$

with the body forces $\boldsymbol{f}$ in Ω and traction vector $\boldsymbol{t}$ on $\partial\Omega_2$, ρ as density and the overhead dot in $\dot{\boldsymbol{u}}$ denotes the derivative with respect to time. The dot between two given vectors denotes the dot product, e.g. $\boldsymbol{a} \cdot \boldsymbol{b} = a_i b_j$.
The stress tensor $\boldsymbol{\sigma}$ is considered as an additional independent variable by appealing to the Legendre transformation for the free energy function in Eq. (2.8). The complementary stored energy $\chi(\boldsymbol{\sigma})$ is a function of stress field, in which $\mathbb{C}^{-1}$ is the inverse of the fourth-order elasticity tensor.

$$\psi^e\left(\boldsymbol{\epsilon} - \boldsymbol{\epsilon}^{vp}\right) = \boldsymbol{\sigma} : \left(\boldsymbol{\epsilon} - \boldsymbol{\epsilon}^{vp}\right) - \chi(\boldsymbol{\sigma}); \quad \chi(\boldsymbol{\sigma}) = \frac{1}{2} \boldsymbol{\sigma} : \mathbb{C}^{-1} : \boldsymbol{\sigma} \tag{2.8}$$

From Eq. (2.8) and Eq. (2.3), the Hellinger-Reissner functional $E^{HR}(\boldsymbol{\sigma}, \boldsymbol{u})$ is now written as functional of the stress $\boldsymbol{\sigma}$ and displacement $\mathbf{u}$ fields.

$$E^{HR}(\boldsymbol{\sigma}, \boldsymbol{u}) = \int_{\Omega} \left[\boldsymbol{\sigma} : \left(\boldsymbol{\epsilon} - \boldsymbol{\epsilon}^{vp}\right) - \chi(\boldsymbol{\sigma})\right] \mathrm{d}V - \Pi^{ext}(\boldsymbol{u}) + K(\dot{\boldsymbol{u}}) \tag{2.9}$$

The least action principle can be used to obtain corresponding variational equations of the functional $E^{HR}(\boldsymbol{\sigma}, \boldsymbol{u})$ above, which can be written as equivalent d'Alembert equations (e.g. [Ibrahimbegovic, 2009]) in terms of the virtual displacement $\delta\boldsymbol{u}$, the virtual stress $\delta\boldsymbol{\sigma}$ as follows:

$$\begin{aligned} G_{\boldsymbol{u}}(\boldsymbol{u}, \boldsymbol{\sigma}; \delta\boldsymbol{u}) := \delta_{\boldsymbol{u}} E^{HR} &= \int_{\Omega} \delta\boldsymbol{\epsilon} : \boldsymbol{\sigma} \mathrm{d}V + \int_{\Omega} \delta\boldsymbol{u} \cdot \rho\ddot{\boldsymbol{u}} dV - \int_{\Omega} \delta\boldsymbol{u} \cdot \boldsymbol{f} \mathrm{d}V - \int_{\partial\Omega_2} \delta\boldsymbol{u} \cdot \boldsymbol{t} \mathrm{d}A \quad = 0 \\ G_{\boldsymbol{\sigma}}(\boldsymbol{u}, \boldsymbol{\sigma}; \delta\boldsymbol{\sigma}) := \delta_{\boldsymbol{\sigma}} E^{HR} &= \int_{\Omega} \left(\delta\boldsymbol{\sigma} : \left(\boldsymbol{\epsilon} - \boldsymbol{\epsilon}^{vp}\right) - \delta\boldsymbol{\sigma} : \partial_{\boldsymbol{\sigma}} \chi(\boldsymbol{\sigma})\right) \mathrm{d}V \quad = 0 \end{aligned} \tag{2.10}$$

where the virtual strain $\delta\boldsymbol{\epsilon}$ tensor is defined as $\nabla^s \delta\boldsymbol{u}$ in the same manner of Eq. (2.2) and the symbol $\partial_{\boldsymbol{\sigma}} \chi(\boldsymbol{\sigma})$ denotes the derivative of complementary stored energy with respect to stress field. The corresponding Euler-Lagrange equations can be obtained directly from the variations in Eq. (2.10).

$$\begin{aligned} G_{\boldsymbol{u}}(\boldsymbol{u}, \boldsymbol{\sigma}; \delta\boldsymbol{u}) &= -\int_{\Omega} \delta\boldsymbol{u} \cdot (\operatorname{div} \boldsymbol{\sigma} + \boldsymbol{f} - \rho\ddot{\boldsymbol{u}}) \mathrm{d}V \quad = 0 \Rightarrow \quad \operatorname{div} \boldsymbol{\sigma} + \boldsymbol{f} = \rho\ddot{\boldsymbol{u}} \\ G_{\boldsymbol{\sigma}}(\boldsymbol{u}, \boldsymbol{\sigma}; \delta\boldsymbol{\sigma}) &= \int_{\Omega} \delta\boldsymbol{\sigma} : \left(\boldsymbol{\epsilon} - \boldsymbol{\epsilon}^{vp} - \partial_{\boldsymbol{\sigma}} \chi(\boldsymbol{\sigma})\right) \mathrm{d}V \quad = 0 \Rightarrow \quad \boldsymbol{\epsilon} - \boldsymbol{\epsilon}^{vp} = \partial_{\boldsymbol{\sigma}} \chi(\boldsymbol{\sigma}) \end{aligned} \tag{2.11}$$

We can appeal to the second law of thermodynamics by means of the Clausius-Duhem inequality to guarantee the thermodynamical admissibility of the constitutive relations

$$\mathcal{D}^{vp} = \boldsymbol{\sigma} : \dot{\boldsymbol{\epsilon}} - \dot{\psi}^e = \boldsymbol{\sigma} : \dot{\boldsymbol{\epsilon}}^{vp} \quad \geq 0 \tag{2.12}$$

where $\mathcal{D}^{vp}$ denotes the visco-plastic dissipation. In principle, all the stress values are admissible, but those outside the elastic domain are penalized by an additional term $P(\cdot)$ directly proportional to the penalty factor $1/\eta$ (with η as the viscosity coefficient depending on material property). The modified visco-plastic dissipation D_{η}^{vp} is now written as follows

$$-D_{\eta}^{vp}[\boldsymbol{\sigma}] = -\boldsymbol{\sigma} : \dot{\boldsymbol{\epsilon}}^{vp} + \frac{1}{\eta} P(\phi(\boldsymbol{\sigma})) \tag{2.13}$$

The simplest choice of the penalty term is a quadratic functional $P(\cdot)$ placing higher penalty on the stress states which are further outside the elastic domain.

$$P(\phi(\boldsymbol{\sigma})) = \begin{cases} \frac{1}{2}\phi(\boldsymbol{\sigma})^2; & \phi(\boldsymbol{\sigma}) \geq 0 \\ 0; & \phi(\boldsymbol{\sigma}) < 0 \end{cases} \Rightarrow \frac{d}{d\phi} P(\phi(\boldsymbol{\sigma})) =< \phi(\boldsymbol{\sigma}) > \tag{2.14}$$

where $< \cdot >$ is the Macauley parenthesis, which is defined as:

$$< \phi >:= (\phi(\boldsymbol{\sigma}) + |\phi(\boldsymbol{\sigma})|)/2 = \begin{cases} \phi(\boldsymbol{\sigma}); & \phi(\boldsymbol{\sigma}) \geq 0 \\ 0; & \phi(\boldsymbol{\sigma}) < 0 \end{cases} \tag{2.15}$$

The evolution of visco-plasticity can be derived by means of the principle of maximum visco-plastic dissipation. From all possible states $\boldsymbol{\sigma}^*$ satisfying the yield criterion $\phi(\boldsymbol{\sigma^*}) \geq 0$, the one $\boldsymbol{\sigma}$ that maximizes visco-plastic dissipation D_η^{vp} is the solution. This problem can also be written as constrained minimization problem.

$$D_\eta^{vp}(\boldsymbol{\sigma}) = \max_{\phi(\boldsymbol{\sigma}^*)\geq 0} \left[D_\eta^{vp}(\boldsymbol{\sigma}^*)\right] \Leftrightarrow -D_\eta^{vp}(\boldsymbol{\sigma}) = \min_{\phi(\boldsymbol{\sigma}^*)\geq 0} \left[-D_\eta^{vp}(\boldsymbol{\sigma}^*)\right] \tag{2.16}$$

The Kuhn-Tucker optimality conditions for the minimization problem defined in the above equation lead to the evolution equation of visco-plastic strain.

$$\mathbf{0} = \frac{\partial D_\eta^{vp}(\boldsymbol{\sigma})}{\partial \boldsymbol{\sigma}} := \frac{\partial[-\boldsymbol{\sigma} : \dot{\boldsymbol{\epsilon}}^{vp} + \frac{1}{\eta} P(\phi(\boldsymbol{\sigma}))]}{\partial \boldsymbol{\sigma}} = -\dot{\boldsymbol{\epsilon}}^{vp} + \frac{1}{\eta} < \phi > \frac{\partial \phi}{\partial \boldsymbol{\sigma}} \tag{2.17}$$

Hence, the rate of visco-plastic strain is written as

$$\dot{\boldsymbol{\epsilon}}^{vp} = \frac{1}{\eta} < \phi > \frac{\partial \phi}{\partial \boldsymbol{\sigma}} =: \boldsymbol{\beta}(\boldsymbol{\sigma}); \quad \frac{\partial \phi}{\partial \boldsymbol{\sigma}} = \frac{3}{\sigma_y^2} \mathrm{dev}(\boldsymbol{\sigma}) \tag{2.18}$$

3 Numerical implementation of visco-plasticity problem

In order to provide the solution for the system of differential equations in Eqs. (2.11) and (2.18) above, the physical domain is discretized via the finite element approximation, while the nonlinear dynamic response is obtained by means of a proposed time-stepping scheme. The main computational task of such a procedure is to calculate the values of the nodal variables and interpolation parameters over a single time interval, which is discussed further in this section.

3.1 Finite element approach

The stress and displacement fields are interpolated independently. At time $t_{n+1/2}$, the displacement field $\boldsymbol{u}_{n+1/2}$ and acceleration field $\ddot{\boldsymbol{u}}_{\boldsymbol{n+1/2}}$ are interpolated from nodal displacement $\boldsymbol{d}_{n+1/2}$ and nodal acceleration $\boldsymbol{a}_{n+1/2}$ vectors via shape function $\boldsymbol{N}$ matrix, respectively.

$$\boldsymbol{u}_{n+1/2} = \boldsymbol{N}\boldsymbol{d}_{n+1/2}; \quad \ddot{\boldsymbol{u}}_{n+1/2} = \boldsymbol{N}\boldsymbol{a}_{n+1/2}$$

The corresponding strain approximation can be derived from displacement field as follows

$$\boldsymbol{\epsilon}_{n+1/2} = \boldsymbol{B}\boldsymbol{d}_{n+1/2}; \quad \boldsymbol{B} = \nabla^s \boldsymbol{N}$$

Meanwhile, the stress field in each element is interpolated directly using a complete linear polynomial $\boldsymbol{S}$ matrix, which is similar to the stress interpolation [Pian and Sumihara, 1984, Wilson and Ibrahimbegovic, 1990] in terms of stress interpolation parameters $\boldsymbol{\tau}_{n+1/2}$ matrix.

$$\boldsymbol{\sigma}_{n+1/2} = \mathbf{S}\boldsymbol{\tau}_{n+1/2}$$

For convenience, the index n+1/2 for the obvious terms is only shown where it is needed. From Eq. (2.10), the discretized weak forms for a typical element Ω^e are written in the matrix forms as follows.

$$\begin{aligned} G^e_{\boldsymbol{u}} &= \delta \boldsymbol{d}^T \left[\int_{\Omega^e} \boldsymbol{B}^T \boldsymbol{S} \boldsymbol{\tau} \mathrm{d}V + \int_{\Omega^e} \rho \mathbf{N}^T \mathbf{N} \boldsymbol{a} dV - \int_{\Omega^e} \boldsymbol{N}^T \boldsymbol{f} \mathrm{d}V - \int_{\partial \Omega^e_2} \boldsymbol{N}^T \boldsymbol{t} \mathrm{d}A \right] &= 0 \\ G^e_{\boldsymbol{\sigma}} &= \delta \boldsymbol{\tau}^T \int_{\Omega^e} \boldsymbol{S}^T \left(\boldsymbol{B}\boldsymbol{d} - \boldsymbol{\epsilon}^{vp} - \partial_{\boldsymbol{\sigma}} \chi(\boldsymbol{\sigma}) \right) \mathrm{d}V &= 0 \end{aligned} \tag{3.1}$$

The linearisation of the first equation Eq. (3.1a) in discretized weak form yields

$$\begin{aligned} \mathrm{Lin}[G^e_{\boldsymbol{u}}] &= G^e_{\boldsymbol{u}}(\boldsymbol{\tau}, \boldsymbol{u}) + \Delta G^e_{\boldsymbol{u}}(\Delta\boldsymbol{\tau}, \Delta\boldsymbol{u}) \\ \Delta G^e_{\boldsymbol{u}}(\Delta\boldsymbol{\tau}, \Delta\boldsymbol{u}) &= \delta \boldsymbol{d}^T \left[\int_{\Omega^e} \boldsymbol{B}^T \boldsymbol{S} \mathrm{d}V \Delta\boldsymbol{\tau} + \eta \int_{\Omega^e} \rho \mathbf{N}^T \mathbf{N} dV \Delta \boldsymbol{d} \right] \end{aligned} \tag{3.2}$$

By considering that the interpolation parameters of virtual fields can be picked arbitrarily, we can obtain the discrete form of the equilibrium equations

$$\begin{aligned} \boldsymbol{r}^{e,(i+1)}_{u,n+1/2}(\boldsymbol{\tau}, \boldsymbol{u}) &= \boldsymbol{r}^{e,(i)}_{u,n+1/2}(\boldsymbol{\tau}, \boldsymbol{u}) + \Delta \boldsymbol{r}^{e,(i)}_{u,n+1/2}(\Delta\boldsymbol{\tau}, \Delta\boldsymbol{u}) = \mathbf{0} \\ \boldsymbol{r}^{e,(i)}_{u,n+1/2}(\cdot) &:= \underbrace{\int_{\Omega^e} \boldsymbol{B}^T \boldsymbol{S} \boldsymbol{\tau}^{e,(i)}_{n+1/2} \mathrm{d}V + \int_{\Omega^e} \rho \mathbf{N}^T \mathbf{N} \boldsymbol{a}^{e,(i)}_{n+1/2} dV}_{\mathbf{f}^{int}_{n+1/2}} \\ &\quad \underbrace{- \int_{\Omega^e} \boldsymbol{N}^T \boldsymbol{f}^{e,(i)}_{n+1/2} \mathrm{d}V + \int_{\partial\Omega^e_2} \boldsymbol{N}^T \boldsymbol{t}^{e,(i)}_{n+1/2} \mathrm{d}A}_{\mathbf{f}^{ext}_{n+1/2}} \\ \Delta \boldsymbol{r}^{e,(i)}_{u,n+1/2}(\cdot) &:= \mathbf{F}^{e,T} \Delta \boldsymbol{\tau}^{e,(i)}_{n+1/2} + \eta \mathbf{M}^e \Delta \boldsymbol{d}^{e,(i)}_{n+1/2} \\ \mathbf{F}^e &:= \int_{\Omega^e} \boldsymbol{S}^T \boldsymbol{B} \mathrm{d}V \\ \mathbf{M}^e &:= \int_{\Omega^e} \rho \mathbf{N}^T \mathbf{N} dV; \ \eta = \partial \boldsymbol{a}_{n+1/2} / \partial \boldsymbol{d}_{n+1/2} \end{aligned} \tag{3.3}$$

The linearization of Eq. (3.1b) in discretized weak form leads to

$$\mathrm{Lin}[G^e_{\boldsymbol{\sigma}}] = G^e_{\boldsymbol{\sigma}}(\boldsymbol{\tau}, \boldsymbol{u}) + \Delta G^e_{\boldsymbol{\sigma}}(\Delta\boldsymbol{\tau}, \Delta\boldsymbol{u}) \tag{3.4}$$

In general, the set of governing equations can be computed with any selected value of $\alpha \in [0, 1]$. However, here we choose the second-order mid-point scheme, by selecting $\alpha = 1/2$.

$$\begin{aligned} \boldsymbol{\sigma}_{n+\alpha} &= (1-\alpha)\boldsymbol{\sigma}_n + \alpha \boldsymbol{\sigma}_{n+1} \, ; \, \alpha = 1/2 \\ \dot{\boldsymbol{\epsilon}}^{vp}_{n+\alpha} &= \boldsymbol{\beta}(\boldsymbol{\sigma}_{n+\alpha}) \Rightarrow \boldsymbol{\epsilon}^{vp}_{n+1/2} = \boldsymbol{\epsilon}^{vp}_n + \frac{\Delta t}{2} \boldsymbol{\beta}(\boldsymbol{\sigma}_{n+1/2}) \\ \partial_{\boldsymbol{\sigma}} \chi(\boldsymbol{\sigma}) &= \mathbf{C}^{-1} : \boldsymbol{\sigma} \end{aligned} \tag{3.5}$$

From the above auxiliary results, the variation $\Delta G^e_{\boldsymbol{\sigma}}(\cdot)$ are derived as follows

$$\begin{aligned} \Delta G^e_{\boldsymbol{\sigma}}(\Delta\boldsymbol{\tau}, \Delta\boldsymbol{u}) &= \delta \boldsymbol{\tau}^T \left[\int_{\boldsymbol{\Omega}^e} \boldsymbol{S}^T \mathbf{B} \mathrm{d}V \Delta \mathbf{d}_{n+1/2} - \int_{\boldsymbol{\Omega}^e} \boldsymbol{S}^T \mathbf{D}^{vp}_{n+1/2} \boldsymbol{S} \mathrm{d}V \Delta \boldsymbol{\tau}_{n+1/2} \right] \\ \mathbf{D}^{vp}_{n+1/2} &:= \frac{\Delta t}{2} \boldsymbol{\beta}^{'}(\boldsymbol{\sigma}_{n+1/2}) + \mathbf{C}^{-1} \\ \boldsymbol{\beta}^{'}(\boldsymbol{\sigma}_{n+1/2}) &= \partial \boldsymbol{\beta}(\boldsymbol{\sigma}_{n+1/2}) / \partial \boldsymbol{\sigma}_{n+1/2} \end{aligned} \tag{3.6}$$

Similarly we also notice that $\delta\boldsymbol{\tau}^T$ is arbitrary virtual stress state so the local governing equation inside a discrete element Ω^e is derived as follows

$$\begin{aligned}
\boldsymbol{h}^{e,(i+1)}_{n+1/2}(\boldsymbol{\tau},\boldsymbol{u}) &= \boldsymbol{h}^{e,(i)}_{n+1/2}(\boldsymbol{\tau},\boldsymbol{u}) + \Delta\boldsymbol{h}^{e,(i)}_{n+1/2}(\Delta\boldsymbol{\tau},\Delta\boldsymbol{u}) = \mathbf{0} \\
\boldsymbol{h}^{e,(i)}_{n+1/2}(\cdot) &:= \int_{\boldsymbol{\Omega}^e} \boldsymbol{S}^T\mathbf{B}\mathrm{d}V\mathbf{d}^{(i)}_{n+1/2} - \int_{\boldsymbol{\Omega}^e} \boldsymbol{S}^T\left(\boldsymbol{\epsilon}^{vp,(i)}_{n+1/2} + \partial_{\boldsymbol{\sigma}}\chi(\boldsymbol{\sigma}^{(i)}_{n+1/2})\right)\mathrm{d}V \\
\Delta\boldsymbol{h}^{e,(i)}_{n+1/2}(\cdot) &:= \mathbf{F}^e\Delta\boldsymbol{d}^{e,(i)}_{n+1/2} - \mathbf{H}^{e,(i)}_{n+1/2}\Delta\boldsymbol{\tau}^{e,(i)}_{n+1/2} \\
\mathbf{H}^e_{n+1/2} &:= \int_{\boldsymbol{\Omega}^e} \boldsymbol{S}^T\mathbf{D}^{vp}_{n+1/2}\boldsymbol{S}\mathrm{d}V
\end{aligned} \tag{3.7}$$

At this point, one can establish the full system of governing equations, in which both nodal displacement and stress are unknown variables.

$$\begin{bmatrix} \mathbb{A}^{nel}_{e=1}\mathbf{F}^{e,T} & \mathbb{A}^{nel}_{e=1}\eta\mathbf{M}^e \\ -\mathbf{H}^e_{n+1/2} & \mathbf{F}^e \end{bmatrix} \begin{bmatrix} \Delta\boldsymbol{\tau}^{e,(i)}_{n+1/2} \\ \Delta\boldsymbol{d}^{e,(i)}_{n+1/2} \end{bmatrix} = - \begin{bmatrix} \mathbb{A}^{nel}_{e=1}\boldsymbol{r}^{e,(i)}_{u,n+1/2}(\cdot) \\ \boldsymbol{h}^{e,(i)}_{n+1/2}(\cdot) \end{bmatrix} \tag{3.8}$$

In the way of programming this problem in an open development platform (such as FEAP-Finite Element Analysis Program) [Taylor, 2014], it is necessary to condense the previous system so that only nodal displacement is the unknown field. The stress field would be computed correspondingly from the displacement fields. From Eq. (3.8b), the stress state in each element can be rewritten as

$$\Delta\boldsymbol{\tau}^e_{n+1/2} = \mathbf{H}^{e,-1}_{n+1/2}\boldsymbol{h}^{e,(i)}_{n+1/2}(\cdot) + \mathbf{H}^{e,-1}_{n+1/2}\mathbf{F}^e\Delta\boldsymbol{d}^e_{n+1/2} \tag{3.9}$$

Substituting the above equation into Eq. (3.3a) yields the condensed system of equations, which depends only on the incremental displacements at time step $t_{n+1/2}$.

$$\begin{aligned}
&\boldsymbol{r}^{e,(i)}_{u,n+1/2}(\cdot) + \mathbf{F}^{e,T}\left[\mathbf{H}^{e,-1}_{n+1/2}\boldsymbol{h}^{e,(i)}_{n+1/2}(\cdot) + \mathbf{H}^{e,-1}_{n+1/2}\mathbf{F}^e\Delta\boldsymbol{d}^{e,(i)}_{n+1/2}\right] + \eta\mathbf{M}^e\Delta\boldsymbol{d}^{e,(i)}_{n+1/2} &&= \mathbf{0} \\
\Leftrightarrow &\left[\boldsymbol{r}^{e,(i)}_{u,n+1/2}(\cdot) + \mathbf{F}^{e,T}\mathbf{H}^{e,-1}_{n+1/2}\boldsymbol{h}^{e,(i)}_{n+1/2}(\cdot)\right] + \left[\mathbf{F}^{e,T}\mathbf{H}^{e,-1}_{n+1/2}\mathbf{F}^e + \eta\mathbf{M}^e\right]\Delta\boldsymbol{d}^{e,(i)}_{n+1/2} &&= \mathbf{0}
\end{aligned} \tag{3.10}$$

Assembling each element contributions over entire discrete domain yields the governing equation of system in matrix form.

$$\begin{aligned}
\mathbb{A}^{nel}_{e=1}\left[\left(\boldsymbol{F}^{e,T}_{n+1/2}\mathbf{H}^{e,-1}_{n+1/2}\boldsymbol{F}^e + \eta\mathbf{M}^e\right)\Delta\boldsymbol{d}^{e,(i)}_{n+1/2}\right] &= -\mathbb{A}^{nel}_{e=1}\left[\boldsymbol{r}^{e,(i)}_{u,n+1/2} + \mathbf{F}^{e,T}\mathbf{H}^{e,-1}_{n+1/2}\boldsymbol{h}^{e,(i)}_{n+1/2}\right] \\
\Leftrightarrow \boldsymbol{K}^{eff,(i)}_{n+1/2}\Delta\boldsymbol{d}^{(i)}_{n+1/2} &= -\boldsymbol{R}^{(i)}_{n+1/2}
\end{aligned} \tag{3.11}$$

In each iteration, the step of displacement is computed via Eq. (3.11). Subsequently, the step of stress is computed at the level of each element from equation Eq. (3.9). The stress and displacement fields are correspondingly updated after each computational iteration of Newton-Raphson method.

$$\begin{aligned}
\boldsymbol{\tau}^{(i+1)}_{n+1/2} &= \boldsymbol{\tau}^{(i)}_{n+1/2} + \Delta\boldsymbol{\tau}^{(i)}_{n+1/2} \\
\boldsymbol{d}^{(i+1)}_{n+1/2} &= \boldsymbol{d}^{(i)}_{n+1/2} + \Delta\boldsymbol{d}^{(i)}_{n+1/2}
\end{aligned} \tag{3.12}$$

3.2 Energy conserving scheme

An energy conserving (EC) scheme is developed to guarantee the stability of the computation over long period for visco-plasticity problem. To achieve the second-order accurate $O(\Delta t^3)$ solution [Artioli et al., 2007], the mid-point time integration scheme is employed. For enforcing the second-order accuracy in visco-plasticity, we must simultaneously integrate visco-plastic

deformation with both displacement and stress, as opposed to the operator split algorithm ([Ibrahimbegovic et al., 1998], [Ibrahimbegovic, 2009]) that separates the integration of these two and thus reduces the time-stepping scheme to first order (e.g. [Chorin et al., 1978]). Accordingly, the nodal velocity $\mathbf{v}_{n+1/2}$ and acceleration $\mathbf{a}_{n+1/2}$ at the time step $t_{n+1/2}$ can be formulated in the form of nodal displacement and velocity.

$$\begin{aligned} \mathbf{v}_{n+1/2} &= (\boldsymbol{d}_{n+1} - \boldsymbol{d}_n)/\Delta t \\ \boldsymbol{a}_{n+1/2} &= (\mathbf{v}_{n+1} - \mathbf{v}_n)/\Delta t \end{aligned} \tag{3.13}$$

The increment of displacement field within an interval of time step is computed by using the mid-point approximation.

$$\boldsymbol{d}_{n+1} - \boldsymbol{d}_n = \frac{1}{2}\Delta t(\mathbf{v}_{n+1} + \mathbf{v}_n) \tag{3.14}$$

This equation can be formed in an alternative expression showing the simple update of displacement vector.

$$\boldsymbol{d}_{n+1} = \boldsymbol{d}_n + \boldsymbol{u}; \quad \boldsymbol{u} := \frac{1}{2}\Delta t(\mathbf{v}_{n+1} + \mathbf{v}_n) \tag{3.15}$$

The stress state at $t_{n+1/2}$ is selected in the following algorithmic form. This proposal, which is left open at the moment, will be explained shortly.

$$\boldsymbol{\tau}^{alg}_{n+1/2} := \frac{1}{2}(\boldsymbol{\tau}_{n+1} + \boldsymbol{\tau}_n) \tag{3.16}$$

By choosing a test displacement vector $\delta\boldsymbol{d} = \boldsymbol{d}_{n+1} - \boldsymbol{d}_n$, a work done both the internal f_{int} and external f_{ext} can be elaborated from the weak form Eq. (3.3b) of balance equation.

$$(\mathbf{d}_{n+1} - \mathbf{d}_n)^T \mathbf{f}^{int}_{n+1/2} = (\mathbf{d}_{n+1} - \mathbf{d}_n)^T \mathbf{f}^{ext}_{n+1/2}$$

The internal work includes two obvious components including kinetic and potential energy.

$$(\mathbf{d}_{n+1} - \mathbf{d}_n)^T \mathbf{f}^{int}_{n+1/2} = (\mathbf{d}_{n+1} - \mathbf{d}_n)^T \int_\Omega \boldsymbol{B}^T \boldsymbol{S}\boldsymbol{\tau}_{n+1/2} \mathrm{d}V + (\mathbf{d}_{n+1} - \mathbf{d}_n)^T \int_\Omega \rho \mathbf{N}^T \mathbf{N} \boldsymbol{a}_{n+1/2} dV$$

The work done by inertia force can be simplified thanks to results obtained in Eq. (3.13b) and (3.14).

$$\begin{aligned} (\mathbf{d}_{n+1} - \mathbf{d}_n)^T \mathbf{M}\mathbf{a}_{n+1/2} &= \frac{1}{2}(\mathbf{v}_{n+1} + \mathbf{v}_n)^T \mathbf{M}(\mathbf{v}_{n+1} - \mathbf{v}_n) \\ &= \frac{1}{2}\mathbf{v}^T_{n+1}\mathbf{M}\mathbf{v}_{n+1} - \frac{1}{2}\mathbf{v}^T_n\mathbf{M}\mathbf{v}_n \\ &= K_{n+1} - K_n \end{aligned} \tag{3.17}$$

where K_{n+1} is the kinetic energy of system at time t_{n+1}. It is noted that the mass matrix $\mathbf{M}$ is symmetric, so this identity holds $\mathbf{v}^T_{n+1}\mathbf{M}\mathbf{v}_n - \mathbf{v}^T_n\mathbf{M}\mathbf{v}_{n+1} = 0$. In the followings, the subscript $'n+1/2'$ for matrix $\boldsymbol{F}$ and $\boldsymbol{H}$ is dropped for shorter expression. The work done by potential force can be also expressed as a combination of 2 groups.

$$\begin{aligned} (\mathbf{d}_{n+1} - \mathbf{d}_n)^T \mathbf{F}^T \boldsymbol{\tau}_{n+1/2} &= \frac{1}{2}(\mathbf{d}_{n+1} - \mathbf{d}_n)^T \mathbf{F}^T(\boldsymbol{\tau}_{n+1} + \boldsymbol{\tau}_n) \\ &= \left[\frac{1}{2}\mathbf{d}^T_{n+1}\mathbf{F}^T\boldsymbol{\tau}_{n+1} - \frac{1}{2}\mathbf{d}^T_n\mathbf{F}^T\boldsymbol{\tau}_n\right] + \underbrace{\left[\frac{1}{2}\mathbf{d}^T_{n+1}\mathbf{F}^T\boldsymbol{\tau}_n - \frac{1}{2}\mathbf{d}^T_n\mathbf{F}^T\boldsymbol{\tau}_{n+1}\right]}_{L} \end{aligned} \tag{3.18}$$

Since the scalar L has a mix variables from both time step t_n and t_{n+1}, further simplification of L should be elaborated. Via exploiting the equation Eq. (3.7b) with a test stress function

$\delta\boldsymbol{\tau}^T = \boldsymbol{\tau}_{n+1} - \boldsymbol{\tau}_n$, the following identity is derived based on the fact that the matrix $\boldsymbol{H}$ is always symmetric, even when the system goes into visco-plastic regime.

$$\begin{aligned}
&(\boldsymbol{\tau}_{n+1} - \boldsymbol{\tau}_n)^T \left[\mathbf{F}\boldsymbol{d}_{n+1/2} - \mathbf{H}\boldsymbol{\tau}_{n+1/2}\right] && = 0 \\
\Rightarrow &\frac{1}{2}\mathbf{d}_{n+1}^T\mathbf{F}^T\boldsymbol{\tau}_{n+1} - \frac{1}{2}\boldsymbol{\tau}_{n+1}^T\mathbf{H}\boldsymbol{\tau}_{n+1} - \frac{1}{2}\mathbf{d}_n^T\mathbf{F}^T\boldsymbol{\tau}_n + \frac{1}{2}\boldsymbol{\tau}_n^T\mathbf{H}\boldsymbol{\tau}_n && = \underbrace{\frac{1}{2}\mathbf{d}_{n+1}^T\mathbf{F}^T\boldsymbol{\tau}_n - \frac{1}{2}\mathbf{d}_n^T\mathbf{F}^T\boldsymbol{\tau}_{n+1}}_{L}
\end{aligned} \tag{3.19}$$

The matrix $\boldsymbol{H}$ can be decomposed in two matrices, the first one $\boldsymbol{H}^{vp}_{n+1/2}$ is a function of visco-plastic strain rate $\dot{\boldsymbol{\epsilon}}^{vp}_{n+1/2}$ and the other $\boldsymbol{H}^e$ is a function of material elastic modulus. It is clear that the matrix $\boldsymbol{H}^{vp}_{n+1/2}$ vanishes under the elastic regime, where the visco-plastic strain does not evolve ($\dot{\boldsymbol{\epsilon}}^{vp}_{n+1/2} = 0$). With the last identity, Eq. (3.18) can be rewritten.

$$\begin{aligned}
(\mathbf{d}_{n+1} - \mathbf{d}_n)^T \mathbf{F}^T\boldsymbol{\tau}_{n+1/2} &= \frac{1}{2}\mathbf{d}_{n+1}^T\mathbf{F}^T\boldsymbol{\tau}_{n+1} - \frac{1}{2}\mathbf{d}_n^T\mathbf{F}^T\boldsymbol{\tau}_n \\
&+ \frac{1}{2}\mathbf{d}_{n+1}^T\mathbf{F}^T\boldsymbol{\tau}_{n+1} - \frac{1}{2}\boldsymbol{\tau}_{n+1}\mathbf{H}\boldsymbol{\tau}_{n+1} - \frac{1}{2}\mathbf{d}_n^T\mathbf{F}^T\boldsymbol{\tau}_n + \frac{1}{2}\boldsymbol{\tau}_n\mathbf{H}\boldsymbol{\tau}_n \\
&= \underbrace{\mathbf{d}_{n+1}^T\mathbf{F}^T\boldsymbol{\tau}_{n+1} - \frac{1}{2}\boldsymbol{\tau}_{n+1}^T\mathbf{H}^e\boldsymbol{\tau}_{n+1}}_{P_{n+1}} - \underbrace{(\mathbf{d}_n^T\mathbf{F}^T\boldsymbol{\tau}_n - \frac{1}{2}\boldsymbol{\tau}_n^T\mathbf{H}^e\boldsymbol{\tau}_n)}_{P_n} \\
&+ \underbrace{(\frac{1}{2}\boldsymbol{\tau}_n^T\mathbf{H}^{vp}_{n+1/2}\boldsymbol{\tau}_n - \frac{1}{2}\boldsymbol{\tau}_{n+1}^T\mathbf{H}^{vp}_{n+1/2}\boldsymbol{\tau}_{n+1})}_{D^{vp}_{n+1/2}} \\
&= P_{n+1} - P_n + D^{vp}_{n+1/2}
\end{aligned} \tag{3.20}$$

where P_{n+1} is the potential energy of system at time t_{n+1} and $D^{vp}_{n+1/2}$ is the visco-plastic dissipation within an interval of time step. From the above derivation, one can express the balance of the internal energy and external work in following equation.

$$\begin{aligned}
&\underbrace{(K_{n+1} + P_{n+1})}_{E_{n+1}} - \underbrace{(K_n + P_n)}_{E_n} + D^{vp}_{n+1/2} && = \underbrace{(\boldsymbol{d}_{n+1} - \boldsymbol{d}_n)^T\boldsymbol{f}^{ext}_{n+1/2}}_{\Delta W_{n+1/2}} \\
&E_{n+1} - E_n + D^{vp}_{n+1/2} && = \Delta W_{n+1/2}
\end{aligned} \tag{3.21}$$

The symbols E_n and E_{n+1} denote the total energy of system at time step t_n and t_{n+1}, respectively. We can conclude that the proposed algorithmic constitutive equation in Eq. (3.16) would conserve the total energy $E_{n+1} = E_n + \Delta W_{n+1/2}$ for any bounded external loading as long as the system undergoing elastic regime ($D^{vp}_{n+1/2} = 0$). This property is viewed as "unconditionally stable" [Zienkiewicz et al., 2005]. Otherwise, once the system undergoes the visco-plastic regime, the total energy can not be conserved anymore due to the existence of visco-plastic dissipation ($D^{vp}_{n+1/2} \neq 0$). However, this non-negative visco-plastic dissipation is always bounded via the controllable penalty factor as shown in Section 2.

3.3 Energy decaying scheme

An energy decaying (ED) scheme is an alternative approach to control potential instability problems of time-stepping algorithms, with an additional advantage of a providing superior accuracy in stress computations by eliminating the high-frequency noise especially for a set of stiff equations (e.g. see [Ibrahimbegovic and Mamouri, 2002]). The latter implies a large difference between max/min eigenvalues in tangent stiffness, which can also occur in the present case when one part of the domain has turned visco-plastic and the rest still remains elastic. In this case, we will enforce so-called a modified constitutive algorithm with the ability of decaying

contribution of higher frequencies over each interval of time step. Such algorithmic updates for of displacement and stress at time step $t_{n+1/2}$ are represented by modifying the conservative terms, as defined in Eqs. (3.14) and (3.16), with the corresponding dissipative terms:

$$\begin{aligned} \boldsymbol{d}_{n+1} - \boldsymbol{d}_n &:= \frac{\Delta t}{2}(\mathbf{v}_{n+1} + \mathbf{v}_n) + \alpha \Delta t(\mathbf{v}_{n+1} - \mathbf{v}_n) \\ \boldsymbol{\tau}^{alg}_{n+1/2} &:= \frac{1}{2}(\boldsymbol{\tau}_{n+1} + \boldsymbol{\tau}_n) + \beta(\boldsymbol{\tau}_{n+1} - \boldsymbol{\tau}_n) \end{aligned} \tag{3.22}$$

where α and β are the dissipation coefficients, which are typically chosen as $\alpha, \beta \in [0, 0.1]$. The corresponding dissipative correction terms $\alpha\Delta t(\mathbf{v}_{n+1} - \mathbf{v}_n)$ and $\beta(\boldsymbol{\tau}_{n+1} - \boldsymbol{\tau}_n)$ remain typically small, or practically vanish, for low frequency modes with a small difference of successive values within a typical time step; the latter establishes the consistency of the present modification in the spirit of the EC scheme, for the case where high frequency modes are not triggered. Meanwhile, the correction terms are less likely to vanish in high frequency modes, where the corresponding successive values within a time step can be quite significant. Therefore, the energy decaying scheme is only introducing a slight perturbation, which is not likely to fully reduce the scheme performance to the first-order accuracy. With such a choice of algorithmic update of displacement and stress updates, the velocity and stress at time step t_{n+1} take a modified form:

$$\begin{aligned} \mathbf{v}_{n+1} &= \frac{1}{(1/2+\alpha)\Delta t}(\boldsymbol{d}_{n+1} - \boldsymbol{d}_n) - \frac{1/2-\alpha}{1/2+\alpha}\mathbf{v}_n \\ \boldsymbol{\tau}_{n+1} &= \frac{1}{1/2+\beta}\boldsymbol{\tau}^{alg}_{n+1/2} - \frac{1/2-\beta}{1/2+\beta}\boldsymbol{\tau}_n \end{aligned} \tag{3.23}$$

One can apply the same implementation as presented in Section 3.2. The work done by inertia force takes a new form.

$$\begin{aligned} (\mathbf{d}_{n+1} - \mathbf{d}_n)^T \mathbf{M}\mathbf{a}_{n+1/2} &= \frac{1}{2}\mathbf{v}^T_{n+1}\mathbf{M}\mathbf{v}_{n+1} - \frac{1}{2}\mathbf{v}^T_n\mathbf{M}\mathbf{v}_n + \underbrace{\alpha(\mathbf{v}_{n+1} - \mathbf{v}_n)^T\mathbf{M}\,(\mathbf{v}_{n+1} - \mathbf{v}_n)}_{D_{K,n+1/2}} \\ &= K_{n+1} - K_n + D_{K,n+1/2} \end{aligned} \tag{3.24}$$

where $D_{K,n+1/2}$ is the numerical dissipation of kinetic energy within an interval of time step. In the followings, the subscript $'n+1/2'$ for matrix $\boldsymbol{F}$ and $\boldsymbol{H}$ is dropped for shorter expression. The work done by potential force takes a combination form of 3 groups.

$$\begin{aligned} (\mathbf{d}_{n+1} - \mathbf{d}_n)^T \mathbf{F}^T\boldsymbol{\tau}_{n+1/2} &= \frac{1}{2}(\mathbf{d}_{n+1} - \mathbf{d}_n)^T \mathbf{F}^T(\boldsymbol{\tau}_{n+1} + \boldsymbol{\tau}_n) \\ &= \left[\frac{1}{2}\mathbf{d}^T_{n+1}\mathbf{F}^T\boldsymbol{\tau}_{n+1} - \frac{1}{2}\mathbf{d}^T_n\mathbf{F}^T\boldsymbol{\tau}_n\right] + \underbrace{\left[\frac{1}{2}\mathbf{d}^T_{n+1}\mathbf{F}^T\boldsymbol{\tau}_n - \frac{1}{2}\mathbf{d}^T_n\mathbf{F}^T\boldsymbol{\tau}_{n+1}\right]}_{L} \\ &+ \underbrace{\beta(\boldsymbol{\tau}_{n+1} - \boldsymbol{\tau}_n)^T\mathbf{H}(\boldsymbol{\tau}_{n+1} - \boldsymbol{\tau}_n)}_{D_{P,n+1/2}} \end{aligned} \tag{3.25}$$

where $D_{P,n+1/2}$ is the numerical dissipation of potential energy within an interval of time step. The similar identity to the one in Eq. (3.19) can be written as

$$\begin{aligned} &(\boldsymbol{\tau}_{n+1} - \boldsymbol{\tau}_n)^T\left[\mathbf{F}\boldsymbol{d}_{n+1/2} - \mathbf{H}\boldsymbol{\tau}_{n+1/2}\right] &&= 0 \\ \Rightarrow &\frac{1}{2}\mathbf{d}^T_{n+1}\mathbf{F}^T\boldsymbol{\tau}_{n+1} - \frac{1}{2}\boldsymbol{\tau}^T_{n+1}\mathbf{H}\boldsymbol{\tau}_{n+1} - \frac{1}{2}\mathbf{d}^T_n\mathbf{F}^T\boldsymbol{\tau}_n + \frac{1}{2}\boldsymbol{\tau}^T_n\mathbf{H}\boldsymbol{\tau}_n & & \\ &+ \beta(\boldsymbol{\tau}_{n+1} - \boldsymbol{\tau}_n)^T\mathbf{H}(\boldsymbol{\tau}_{n+1} - \boldsymbol{\tau}_n) &&= \underbrace{\frac{1}{2}\mathbf{d}^T_{n+1}\mathbf{F}^T\boldsymbol{\tau}_n - \frac{1}{2}\mathbf{d}^T_n\mathbf{F}^T\boldsymbol{\tau}_{n+1}}_{L} \end{aligned} \tag{3.26}$$

With this identity on hand, the work done by potential force takes a new form.

$$
\begin{aligned}
\left(\mathbf{d}_{n+1}-\mathbf{d}_n\right)^T\mathbf{F}^T\boldsymbol{\tau}_{n+1/2} &= \underbrace{\mathbf{d}_{n+1}^T\mathbf{F}^T\boldsymbol{\tau}_{n+1}-\frac{1}{2}\boldsymbol{\tau}_{n+1}^T\mathbf{H}^e\boldsymbol{\tau}_{n+1}}_{P_{n+1}}-\underbrace{\left(\mathbf{d}_n^T\mathbf{F}^T\boldsymbol{\tau}_n-\frac{1}{2}\boldsymbol{\tau}_n^T\mathbf{H}^e\boldsymbol{\tau}_n\right)}_{P_n}\\
&\quad+\underbrace{\left(\frac{1}{2}\boldsymbol{\tau}_n\mathbf{H}_{n+1/2}^{vp}\boldsymbol{\tau}_n-\frac{1}{2}\boldsymbol{\tau}_{n+1}\mathbf{H}_{n+1/2}^{vp}\boldsymbol{\tau}_{n+1}\right)}_{D_{n+1/2}^{vp}}+\underbrace{\beta(\boldsymbol{\tau}_{n+1}-\boldsymbol{\tau}_n)^T\mathbf{H}(\boldsymbol{\tau}_{n+1}-\boldsymbol{\tau}_n)}_{D_{P,n+1/2}}\\
&= P_{n+1}-P_n+D_{n+1/2}^{vp}+D_{P,n+1/2}
\end{aligned}
\tag{3.27}
$$

From the above derivation, the balance of the internal energy and external work can be formed in following equation.

$$
\begin{aligned}
&\underbrace{\left(K_{n+1}+P_{n+1}\right)}_{E_{n+1}}-\underbrace{\left(K_n+P_n\right)}_{E_n}+D_{n+1/2}^{vp}+\underbrace{D_K+D_P}_{D_{KP,n+1/2}} &&=\underbrace{\left(\mathbf{d}_{n+1}-\mathbf{d}_n\right)^T\mathbf{f}_{n+1/2}^{ext}}_{\Delta W_{n+1/2}}\\
&E_{n+1}-E_n+D_{n+1/2}^{vp}+D_{KP,n+1/2} &&=\Delta W_{n+1/2}
\end{aligned}
\tag{3.28}
$$

where $D_{KP,n+1/2}$ is the numerical dissipation of total energy due to the dissipative constitutive algorithm in Eq. 3.23. It is obvious that switching between energy conserving/decaying schemes can be executed flexibly without changing the main code of user-defined element since the update of displacement and velocity updates can be programmed in a separate subroutine for time-stepping integration algorithm. Additionally, the amount of numerical dissipation is fully controllable via an appropriate selection of dissipation coefficients α and β.

4 Representative numerical examples

In order to illustrate the favorable properties of the newly proposed EC and ED schemes for visco-plastic problem, several numerical simulations are presented and compared against more conventional visco-plasticity approach. All the computations are programmed as a user-defined element in computer code FEAP v8.4, see [Taylor, 2014]. The output data is then post-processed via Matlab scripts for plotting.

The computations are performed for both quasi-static and dynamic pressure loads applied to thick-walled pipe by using the proposed finite element formulation based on Hellinger-Reissner variational pinciple, hybrid-stress interpolations and time-stepping schemes developed for visco-plasticity in the previous section. The computed results are compared against either the exact (analytic) solution in the elastic regime or the available results in visco-plasticity regime [Lubliner, 2008], as well as against the previous study results [Hughes and Taylor, 1978]. Additionally, the performance of the proposed element is compared against the quadrilateral rectangle element embedded B-bar method (Q4/P1).

4.1 Quasi-static loadings

The elasticity and visco-plasticity problem of a pipe under a quasi-static internal pressure is considered. In quasi-static analysis, the inertial term, proportional to mass matrix, is neglected in Eq. (3.8). The pipe is assumed very long compared to the outer radius, so that it is subjected to plane strain constraint with zero deformation along the pipe axis. Thanks to the axisymmetry of this 3D problem, the domain can be discretized by finite elements using the shape functions varying only in r direction. The inner and outer radius of pipe are chosen as $r_1 = 1$ and $r_2 = 2$. The properties of pipe material are listed as: elastic modulus $E = 30.10^6$, Poisson's ratio $\nu = 0.3$, yield stress $\sigma_y = 30.10^3$ and $1/\eta = 10^{-8}$. Regarding the boundary conditions, on

the inner end we apply pressure, while the outer end of the pipe is free of stress. The domain is discretized into 8 such elements, each with 3 nodes and 2 Gauss points as in Fig. 5a in r direction, which provide the second order displacement accuracy. This interpolation be handled with isoparametric elements using quadratic shape functions, see [Ibrahimbegovic, 2009]. Thus, the displacement $\boldsymbol{u}$ matrix and strain $\boldsymbol{\epsilon}$ matrix are functions of nodal displacement $\boldsymbol{d}$ matrix, see [Zienkiewicz et al., 2005].

$$u = \sum_{i=1}^{3} N_i u_i \mapsto \mathbf{u} = \mathbf{N}\mathbf{d}; \quad \begin{bmatrix} \epsilon_r & \epsilon_\theta & \epsilon_z \end{bmatrix} = \begin{bmatrix} \dfrac{\partial u}{\partial r} & \dfrac{u}{r} & 0 \end{bmatrix} \mapsto \boldsymbol{\epsilon} = \mathbf{B}\mathbf{d} \tag{4.1}$$

The elasticity matrix in Eq. (3.5c) is rewritten for axisymmetric and plane strain conditions.

$$\mathbb{C} = \frac{E}{(1+v)(1-2v)} \begin{bmatrix} 1-v & v & v \\ v & 1-v & v \\ v & v & 1-v \end{bmatrix} \tag{4.2}$$

The interpolation of stress field is selected based on the equilibrium equations. The latter, expressed in polar coordinates with zero body forces and plane strain constraint, reduces to:

$$\frac{\partial \sigma_{rr}}{\partial r} + \frac{1}{r}(\sigma_{rr} - \sigma_{\theta\theta}) = 0; \quad \frac{\partial \sigma_{\theta\theta}}{\partial \theta} = 0; \quad \frac{\partial \sigma_{zz}}{\partial z} = 0 \tag{4.3}$$

Since the quadratic shape functions for displacement field in this element result with linear strain field, we choose similarly the corresponding stress approximations. In particular, the stress σ_{rr} should be a linear function to avoid the trivial case that it is a constant and equal to $\sigma_{\theta\theta}$. If the stress σ_{zz} and $\sigma_{\theta\theta}$ are constants in order to satisfy the Eqs. (4.3b,c), they can not satisfy the condition for plane strain $(\sigma_{rr} + \sigma_{\theta\theta})\nu = \sigma_{zz}$. As the result, all of three stress components are selected as linear functions. When the element gets smaller, Eq. (4.3) would be satisfied in a "weak" sense. The chosen approximation for stress field can be interpolated from 6 stress parameters, which become part of unknowns in this problem:

$$\begin{bmatrix} \sigma_{rr} \\ \sigma_{\theta\theta} \\ \sigma_{zz} \end{bmatrix} = \begin{bmatrix} 1 & r & 0 & 0 & 0 & 0 \\ 0 & 0 & 1 & r & 0 & 0 \\ 0 & 0 & 0 & 0 & 1 & r \end{bmatrix} \begin{bmatrix} \tau_1 \\ \tau_2 \\ \tau_3 \\ \tau_4 \\ \tau_5 \\ \tau_6 \end{bmatrix} \Rightarrow \boldsymbol{\sigma} = \mathbf{S}\boldsymbol{\tau} \tag{4.4}$$

All the ingredients of chosen discrete approximations are readily replaced into the theoretical formulation presented in Section 3. The analytical solution of stress field for a pipe under internal pressure p, see [Lubliner, 2008], is given as follows.

$$\sigma_r = \frac{-p}{(r_2/r_1)^2 - 1}\left(\frac{r_2^2}{r^2} - 1\right); \quad \sigma_\theta = \frac{p}{(r_2/r_1)^2 - 1}\left(\frac{r_2^2}{r^2} + 1\right); \quad \sigma_z = \frac{2\nu p}{(r_2/r_1)^2 - 1} \tag{4.5}$$

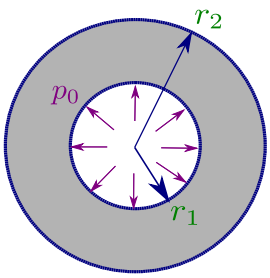

(a) A pipe under internal pressure p_0

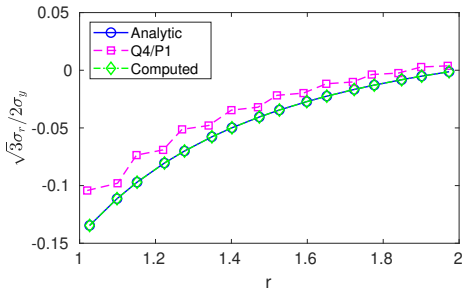

(b) Normalized radial stress σ_r

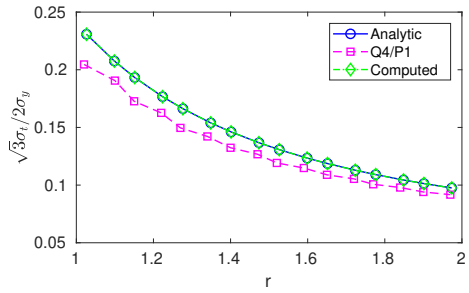

(c) Normalized circumferential stress σ_θ

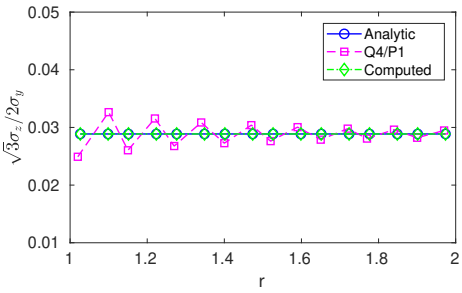

(d) Normalized longitudinal stress σ_z

Fig. 2: Computed stress under elastic regime at $p_0 = 5.10^3$

As shown in Fig. 9a, the pipe under an elastic regime is analyzed by quasi-static analysis, in which the internal pressure p_0 load varies from 0 to 5.10^3 within 100 time steps. A coarse mesh with 8 by 8 elements is required by using enhanced quadrilateral element (Q4/P1) and the result is extracted at Gauss points laying on radial line AB, as shown in Fig. 4a. Meanwhile, a mesh with only 8 elements is adequate by using proposed element, as shown in Fig. 5a. The solution from the proposed element matches exactly the analytic solution while the stress computed by Q4/P1 element show a staggered trend, as shown in Figs. 2b-d. The total time of CPU (by a standard portable computer) to solve this problem is 0.38s by proposed element and 0.86s by Q4/P1 element. It is clear that the proposed element has advanced computational cost with respect to mesh generation and also computational time. To alleviate the high incompressibility constraint and enhance the accuracy of two-dimensional elements in this type of problem, one can also employ other methods such as enhancing displacement gradient by F-bar method (see [Neto et al., 1996, Neto et al., 2005]) and/or generate a finer mesh.

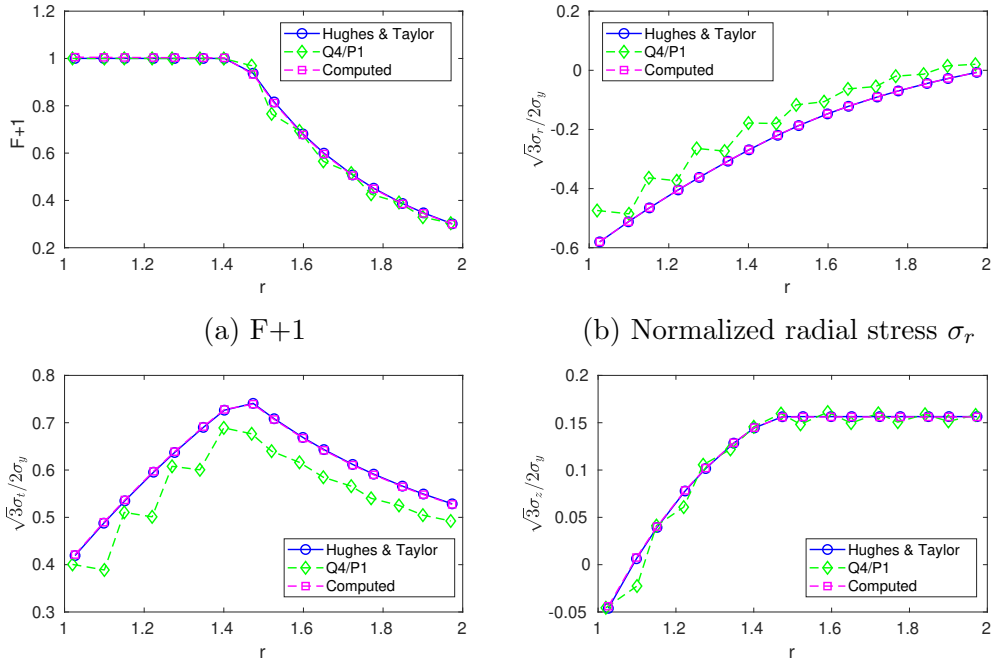

(a) F+1 (b) Normalized radial stress σ_r

(c) Normalized circumferential stress σ_θ (d) Normalized longitudinal stress σ_z

Fig. 3: Computed stress under visco-plastic regime by constant $p_0 = 21.10^3$

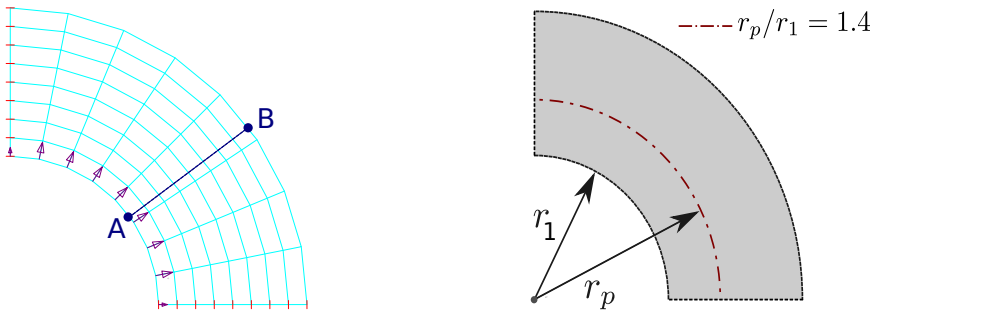

(a) Mesh and boundary condition (b) Separation line at $r_p = 1.4r_1$

Fig. 4: A quarter of a pipe by Q4/P1 element

As shown in Fig. 3, the pipe under a visco-plastic regime is analyzed by quasi-static analysis, in which the internal pressure p_0 load stay constant at the value of 21.10^3. After 15 seconds, the visco-plastic zone develops to the middle of the pipe. This current result is simulated with time step $\Delta t = 10^{-4}$. The zone with $'F + 1 > 1'$ equivalent to $'\phi > 0'$, which has non-zero visco-plastic deformation, corresponds to the region with $r_1 \leq r \leq r_p = 1.4r_1$, as shown in Fig. 3a. Meanwhile the elastic zone is located at $r_p \leq r \leq r_2$. The current solution matches with previous numerical study by Hughes and Taylor, see [Hughes and Taylor, 1978], which is in agreement with the exact solution given by Prager and Hodge with the ratio $r_p/r_1 = 1.4$, see page 271 of [Lubliner, 2008]. Compared to elastic analysis, the similar trend of radial stress can be observed, as shown in Fig. 3b. Meanwhile, the circumferential and longitudinal stresses show clearly two different zones due to the existence of visco-plasticity, as shown in Fig. 3c,d. The stress field is also compared to that from Q4/P1 element under perfectly plastic regime. The location r_p of separation line is the same as that from the proposed element, as shown in Fig. 4b. It is also noticed that the solution from Q4/P1 element show a staggered trend, as shown in Fig. 3b-d. For the proposed element, the visco-plastic problem is solved within 3 iterations under quadratic convergence rate (energy residual up-to 10^{-15}). The proposed

element shows an advanced smooth and accurate stress field compared to Q4/P1 element in the pipe.

4.2 Dynamic loadings

The visco-plastic problem inside selected thick-walled pipes is simulated under dynamic loads. There are two models with different radius for the simulation. The first one has $r_1 = 1$ and $r_2 = 2$ referred as "soft" model, while the other has $r_1 = 5$ and $r_2 = 10$ referred as "stiff" model. The difference between two concerns the corresponding ratio between the smallest and largest eigenvalues of the tangent stiffness. The same number of elements is used to perform the computations for both models. The results presented subsequently for cases 1-3 belong to the "soft" model and for cases 4-6 belong to the "stiff" model. The chosen time step in all simulations is $\Delta t = 10^{-5}$, which is able to capture high frequency response.

Regarding the energy conserving (EC) scheme, only one triangle pulse with a peak of pressure p_0 is introduced to both models as shown in Fig. 5a, which subsequently leads to the free vibration of system. Several cases with different pulse loading duration are examined, as listed in Table 1. Regarding the energy decaying (ED) scheme, an additional pulse of short duration is later introduced into the system. This pulse is applied on end-nodes of each element with opposite direction, as shown in Fig. 5b, in order to activate high frequency modes of the system. The results are extracted at nodes 1, 9 and 17 as shown in Fig. 5a and at elements 1, 4 and 8 as shown in Fig. 5b. Several cases with different values for dissipation factors (α, β) are shown in Table 2.

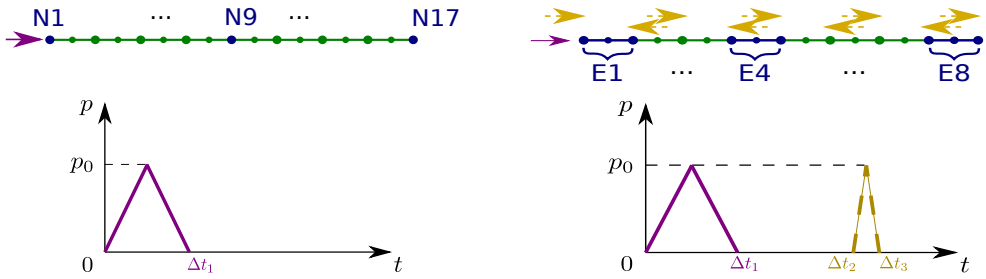

(a) One pulse: EC scheme (b) Two pulses: ED scheme

Fig. 5: Mesh and pressure pulses

Simulation	Model	Case	p_0	Δt_1
Elastic regime	1	1,2,3	21e2	4e-4,6e-4,8e-4
(EC scheme)	2	4,5,6	21e2	4e-4,6e-4,8e-4
Visco-plastic regime	1	1,2,3	42e3	4e-4,6e-4,8e-4
(EC scheme)	2	4,5,6	42e4	4e-4,6e-4,8e-4

Table 1: Load groups for EC scheme

Simulation	Model	Case	p_0	Δt_1	Δt_2	Δt_3	$\alpha = \beta$
Elastic regime	1	1,2,3	21e2	8e-4	30e-4	31e-4	0.01,0.05,0.1
(ED scheme)	2	4,5,6	21e2	8e-4	30e-4	31e-4	0.01,0.05,0.1
Visco-plastic regime	1	1,2,3	42e3	8e-4	30e-4	31e-4	0.01,0.05,0.1
(ED scheme)	2	4,5,6	42e4	8e-4	30e-4	31e-4	0.01,0.05,0.1

Table 2: Load groups for ED scheme

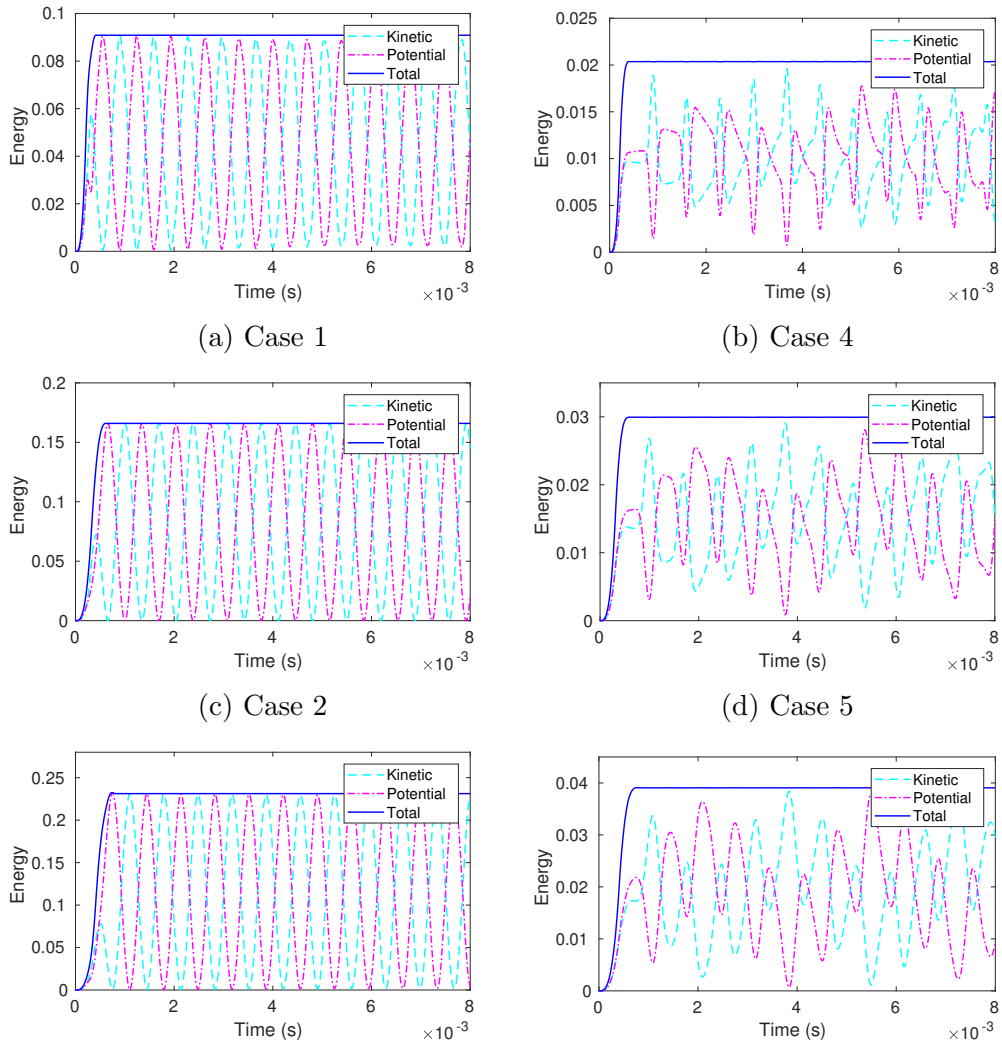

(a) Case 1 (b) Case 4

(c) Case 2 (d) Case 5

(e) Case 3 (f) Case 6

Fig. 6: Energy conserving under elastic regime (EC scheme)

The results in Fig. 6 show that the total internal energy of system is conserved exactly under free vibration. The case 1-3 is from soft model and case 4-5 is from stiff model. After releasing the external load, the total energy of system, including kinetic and potential energies, remains constant and coincides with the external energy introduced to system by the pulse. For example, the total energy of system is around 0.09 in case 1 and 0.02 in case 4, as shown in Figs. 6a,b. Longer duration of loading leads to higher total energy gained by the system. It is noted that these cases are fully under elastic regime without any evolution of visco-plasticity strain. The dynamic response of system including displacement, velocity and stress are recorded at node number 1, 9 and 17, which are, respectively, at the inner radius, in the middle and at the outer radius of the mesh, as shown in Fig. 5a.

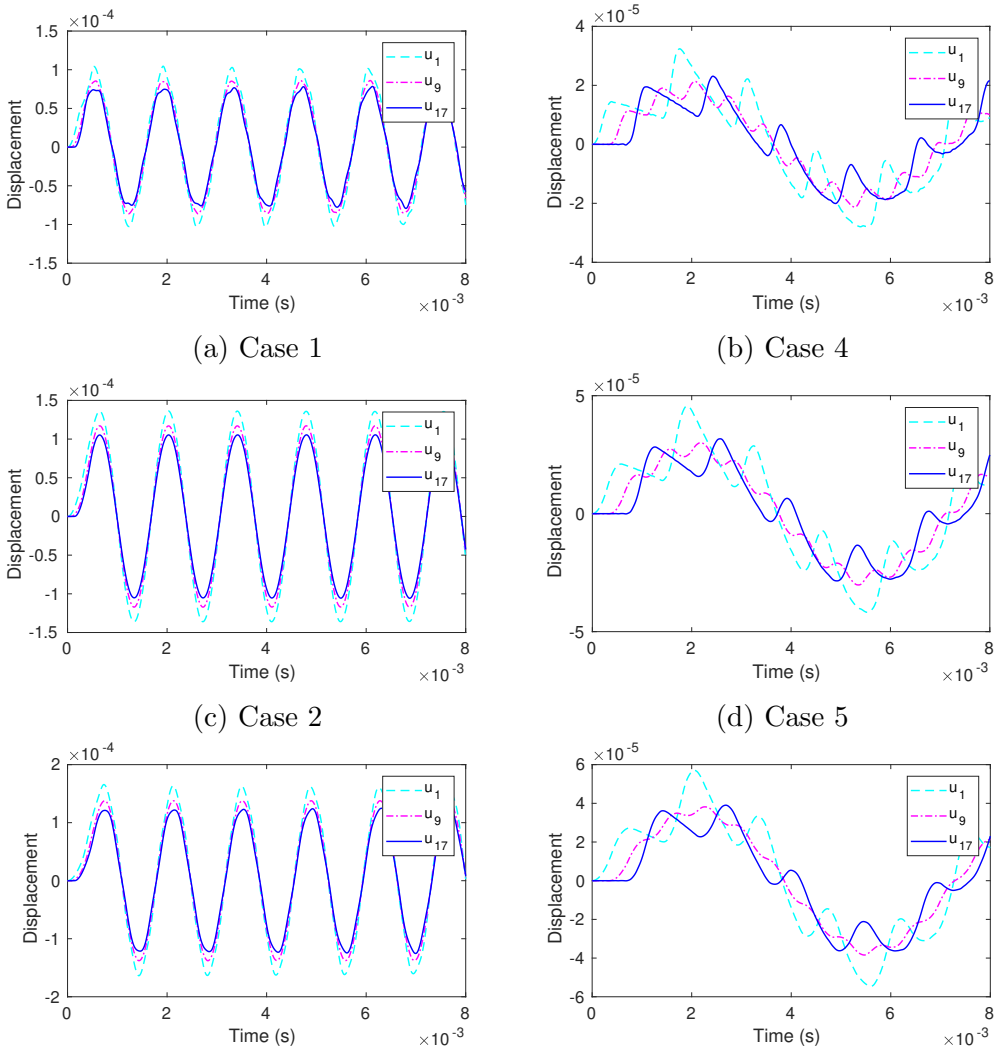

(a) Case 1 (b) Case 4

(c) Case 2 (d) Case 5

(e) Case 3 (f) Case 6

Fig. 7: Displacement under elastic regime (EC scheme)

As shown in Fig. 7, the amplitude of displacement at node 1 is higher than those at other nodes since the pulse is applied at this node. It is noted that the displacement field in soft model is dominated by one frequency, whereas this is no longer the case in stiff model.

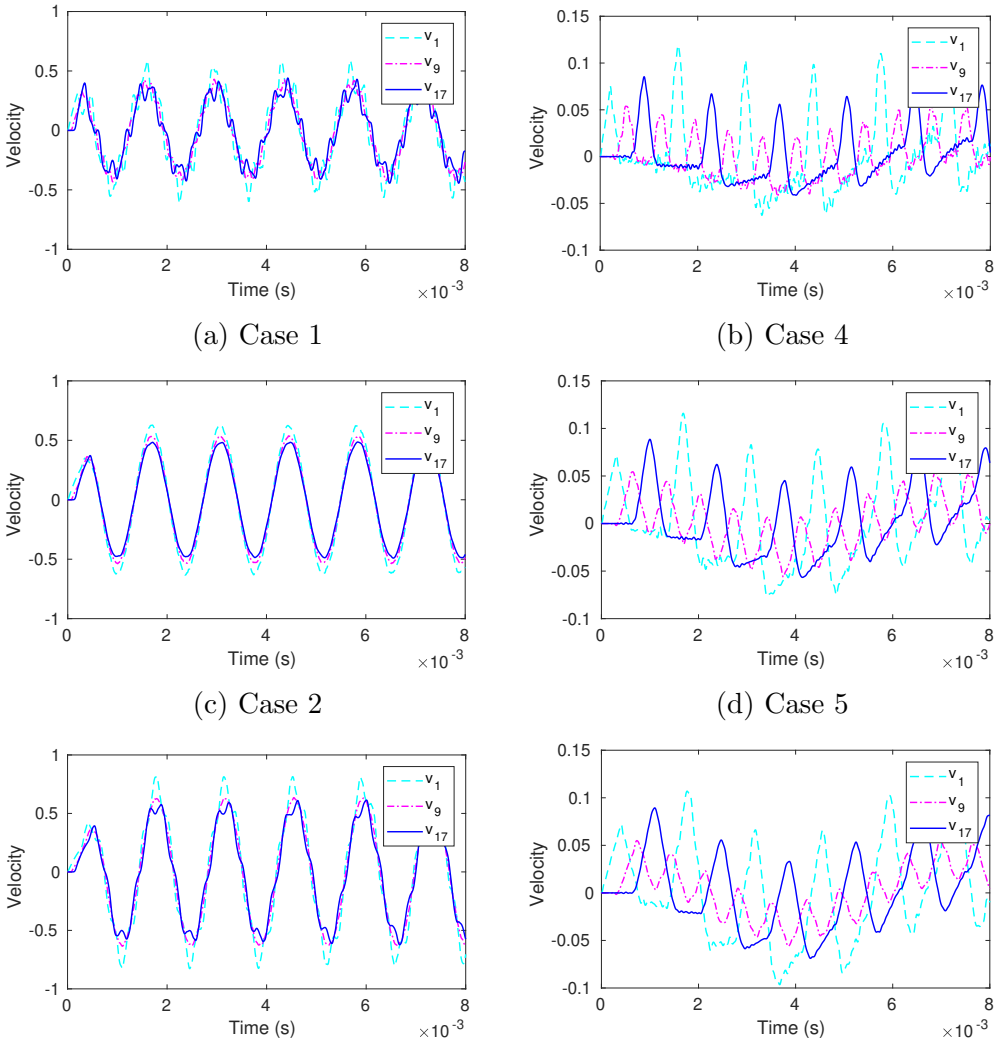

(a) Case 1 (b) Case 4

(c) Case 2 (d) Case 5

(e) Case 3 (f) Case 6

Fig. 8: Velocity under elastic regime (EC scheme)

A similar observation is made regarding the velocity and stress fields, as shown in Figs. 8 and 9, where higher values of absolute displacement leads to higher stress. During the elastic regime, the norm of deviatoric part of largest stress $||\,\mathrm{dev}(\sigma)||$ always remains lower than the critical value $\sqrt{\frac{2}{3}}\sigma_y \approx 24.5 \times 10^3$ (see Eq. (2.6)), which is equivalent to $\phi < 0$.

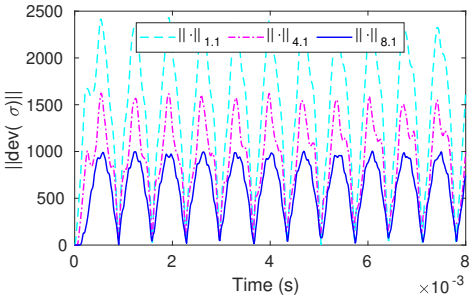

(a) Case 1

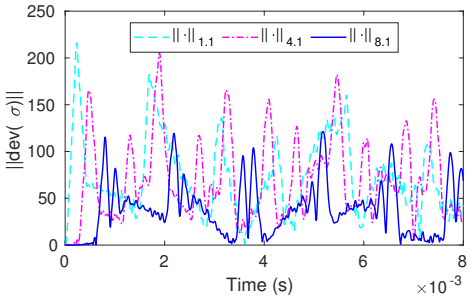

(b) Case 4

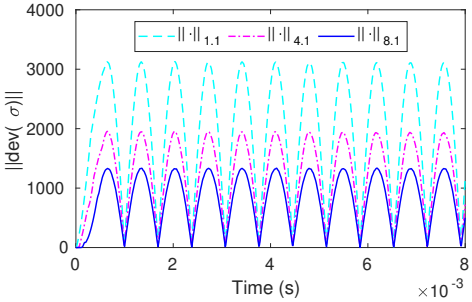

(c) Case 2

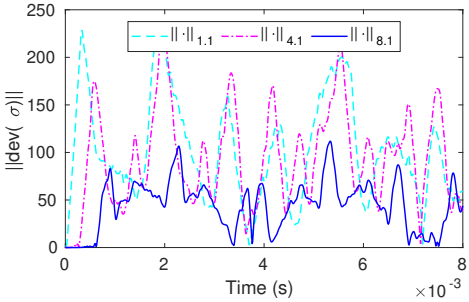

(d) Case 5

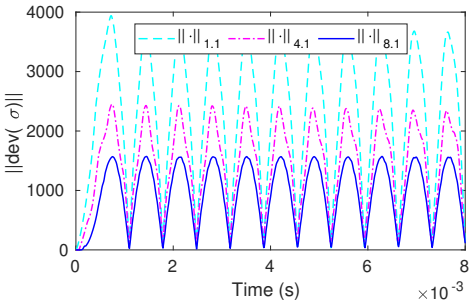

(e) Case 3

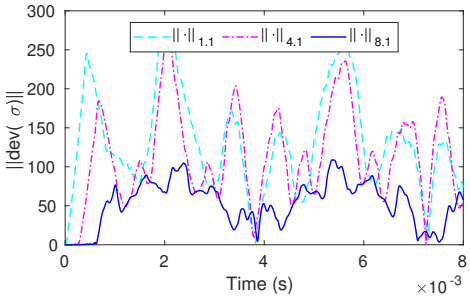

(f) Case 6

Fig. 9: Stress under elastic regime (EC scheme)

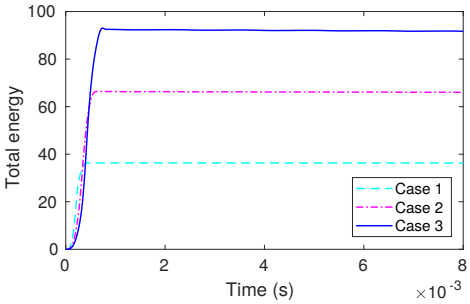

(a) Case 1-3: total energy

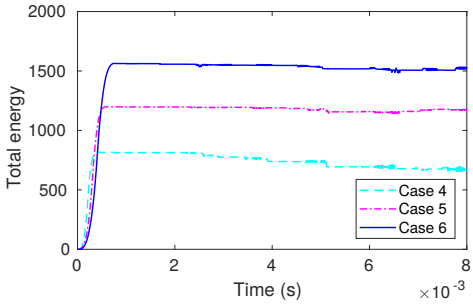

(b) Case 4-6: total energy

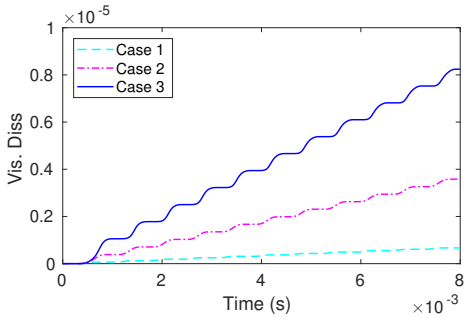

(c) Case 1-3: visco-plastic dissipation

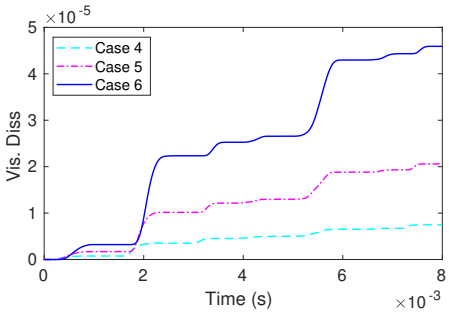

(d) Case 4-6: visco-plastic dissipation

Fig. 10: Energy and dissipation under visco-plastic regime (EC scheme)

The same numerical examples are further examined under visco-plastic regime. Here, higher values of pressure pulse have to be introduced in order to activate visco-plastic regime. In particular, the stiff model requires a higher pulse amplitude compared to the soft model. During visco-plastic regime, the total energy of system is not conserved due to the evolution of visco-plastic dissipation, as shown in Fig. 10. However, since the visco-plastic dissipation remains rather small, the total energy of system is approximately comparable to the total external work after releasing the pulse. For example, the total external work is around 38 in Case 1 and 800 in Case 4, as shown in Figs. 10a,b. The visco-plastic dissipation increases overall; however it stays constant sometimes when there is no excursion in visco-plastic regime. This trend can be explained clearly by corresponding variations of the stress field, as in Fig. 11.

The stresses are extracted from only first Gauss point of elements 1, 4 and 8 (numbered starting from the inner radius), as shown in Fig. 5b. During the period that every element has the value $||\operatorname{dev}(\sigma)|| < \sqrt{\frac{2}{3}}\sigma_y$ (or equivalent to $\phi < 0$), the whole system is under elastic regime and there is no evolution of visco-plastic strain, which keeps the corresponding visco-plastic dissipation constant. By contrast, the visco-plastic dissipation evolves when the yielding criteria is satisfied, precisely $||\operatorname{dev}(\sigma)|| > \sqrt{\frac{2}{3}}\sigma_y$. This energy dissipation depends on type of material in which the viscosity coefficient η is taken into account.

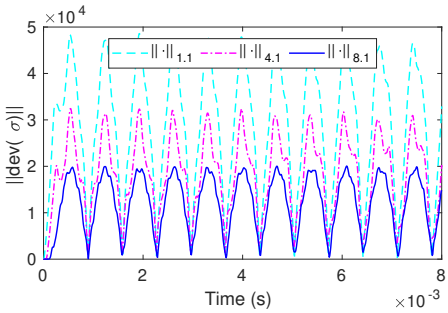

(a) Case 1

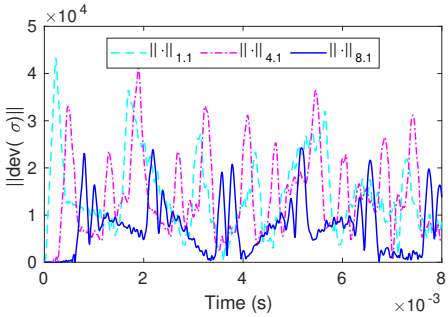

(b) Case 4

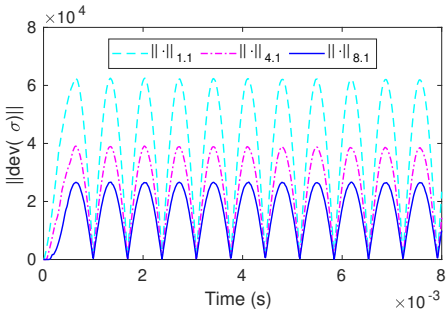

(c) Case 2

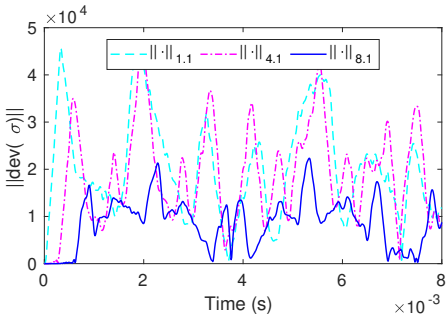

(d) Case 5

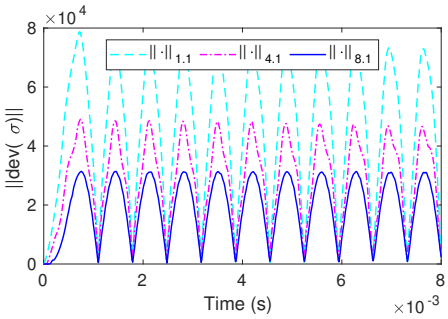

(e) Case 3

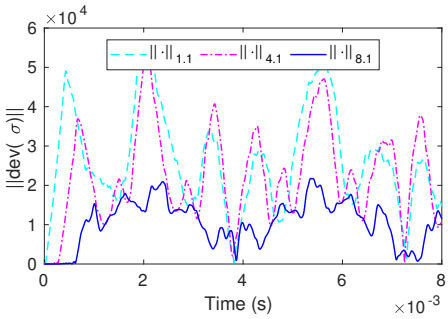

(f) Case 6

Fig. 11: Stress under visco-plastic regime (EC scheme)

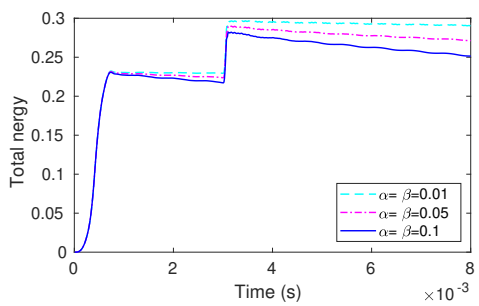

(a) Case 1-3: total energy

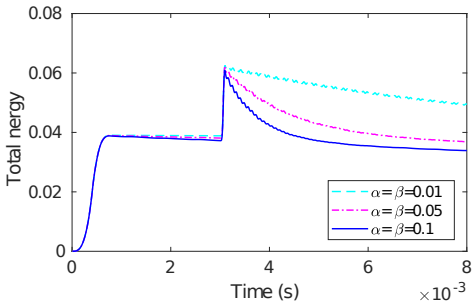

(b) Case 4-6: total energy

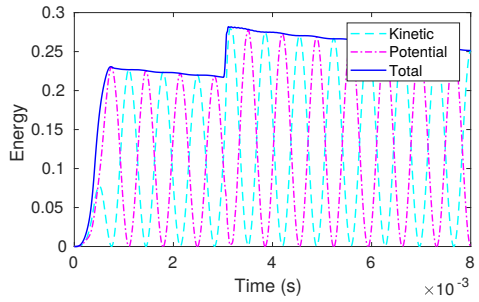

(c) Case 3: energies with $\alpha = \beta = 0.1$

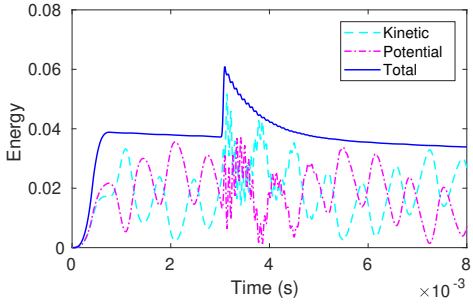

(d) Case 6: energies with $\alpha = \beta = 0.1$

Fig. 12: Energy under elastic regime (ED scheme)

In Fig. 12, we show the total energy of system in the elastic regime, computed by ED scheme. The only dissipation sources are introduced by energy-decaying scheme, where higher frequency dissipation is controlled by dissipation factors α, β that regulate potential and kinetic dissipation energies. In both soft and stiff models, there are 3 cases with different dissipation factors $(\alpha, \beta) \in \{(0.01, 0.01), (0.05, 0.05), (0.1, 0.1)\}$. It is obvious that the dissipative energy increases proportionally with respect to the chosen values of dissipation factors (α, β) as shown in Figs. 12a,b. In case 3 of soft model, the total energy decreases slightly due to the dissipative energy over time as shown in 12c. The same pattern can be better recognized after the injection of high frequency modes contribution produced by the second pulse. This high frequency pulse does not dissipate neither kinetic nor potential energy of the soft model as much as it dissipates in case 6 of the stiff model. The noise generated by the second pulse is dissipated out quickly for both kinetic and potential energies, as shown in Fig. 12d. When dissipation factors (α, β) approach zeros, Figs. 12a,b will agree with Figs. 6e,f in the period before introducing the second pulse at $\Delta t_2 = 30.10^{-3}$.

In Fig. 13, the stresses are taken again in elements 1, 4 and 8 at the Gauss points as in previous simulation. As shown in Figs. 13a,c,e, the second pulse in soft model does not bring much noise to the stress, except for the an obvious effect that it increases the magnitude of stresses. However, the perturbation of high frequency modes can be viewed from cases 4-6 in the stiff model. As shown in Fig. 13f, high frequency stresses are quickly filtered out of the system with $\alpha = \beta = 0.1$, which is faster than the other cases with smaller values of α and β, as shown in Fig. 13b,d.

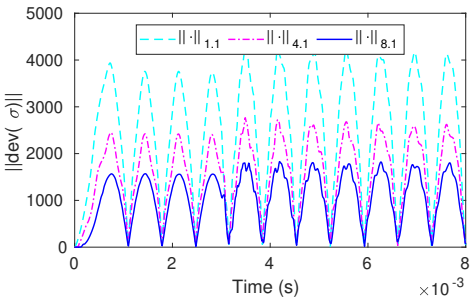

(a) Case 1

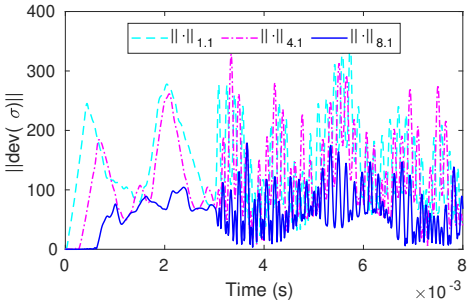

(b) Case 4

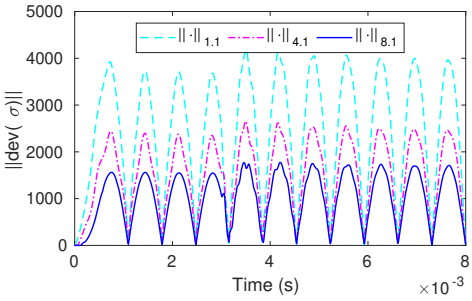

(c) Case 2

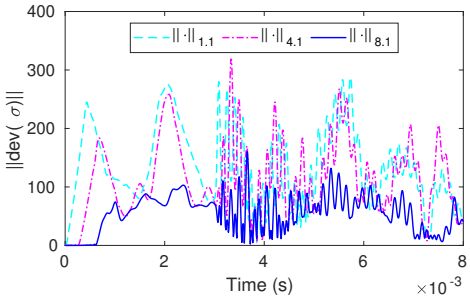

(d) Case 5

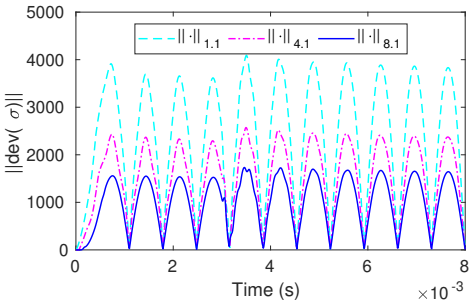

(e) Case 3

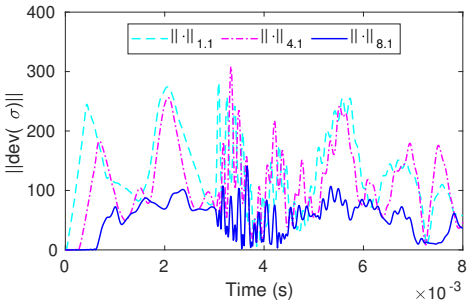

(f) Case 6

Fig. 13: Stress under elastic regime (ED scheme)

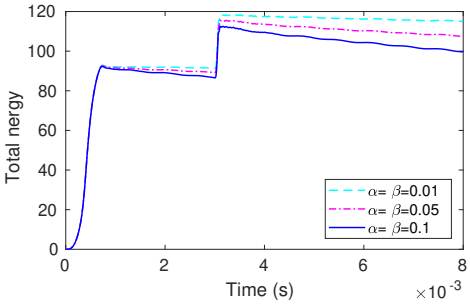

(a) Case 1-3: total energy

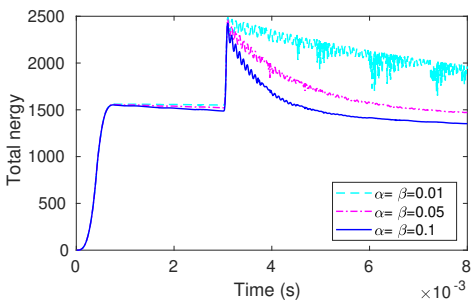

(b) Case 4-6: total energy

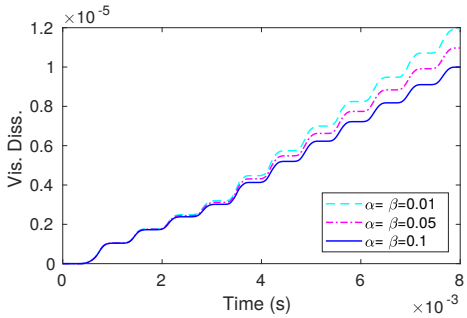

(c) Case 1-3: visco-plastic dissipation

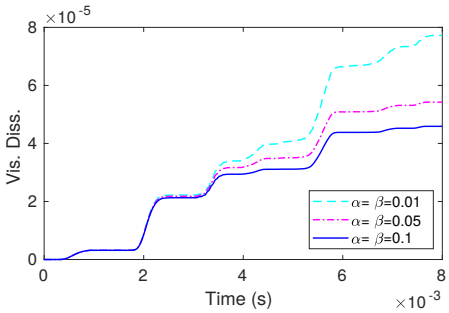

(d) Case 4-6: visco-plastic dissipation

Fig. 14: Energy under visco-plastic regime (ED scheme)

As shown in Fig. 14, the total energy of system under visco-plastic regime are computed by ED scheme. There are in total 3 sources of dissipation, namely visco-plastic dissipation, numerical dissipation of energy-decaying scheme for kinetic and for potential energy. The direct correlation between the higher values of α and β versus resulting numerical dissipation is obviously captured in Figs. 14a and 14b. The visco-plastic dissipation increases in time whenever the system satisfies the yield criteria, as shown in Figs. 14c and 14d. It is recognized that numerical dissipation is much higher than for the visco-plasticity. From the results in Fig. 12a,b and Fig. 14a,b, the trend and relative dissipation of system due to ED scheme is comparable between elastic and visco-plastic regimes.

The stresses are taken again in elements 1, 4 and 8 at the first Gauss points, as presented in Fig. 15. Similar to the previous simulation, the second pulse bring only little noise to the stress in soft model, as shown in Figs. 15a,c,e. The same observation on the energy-decaying on high frequency mode's contribution no longer applies for the stiff model, as shown in Figs. 15b,d,f.

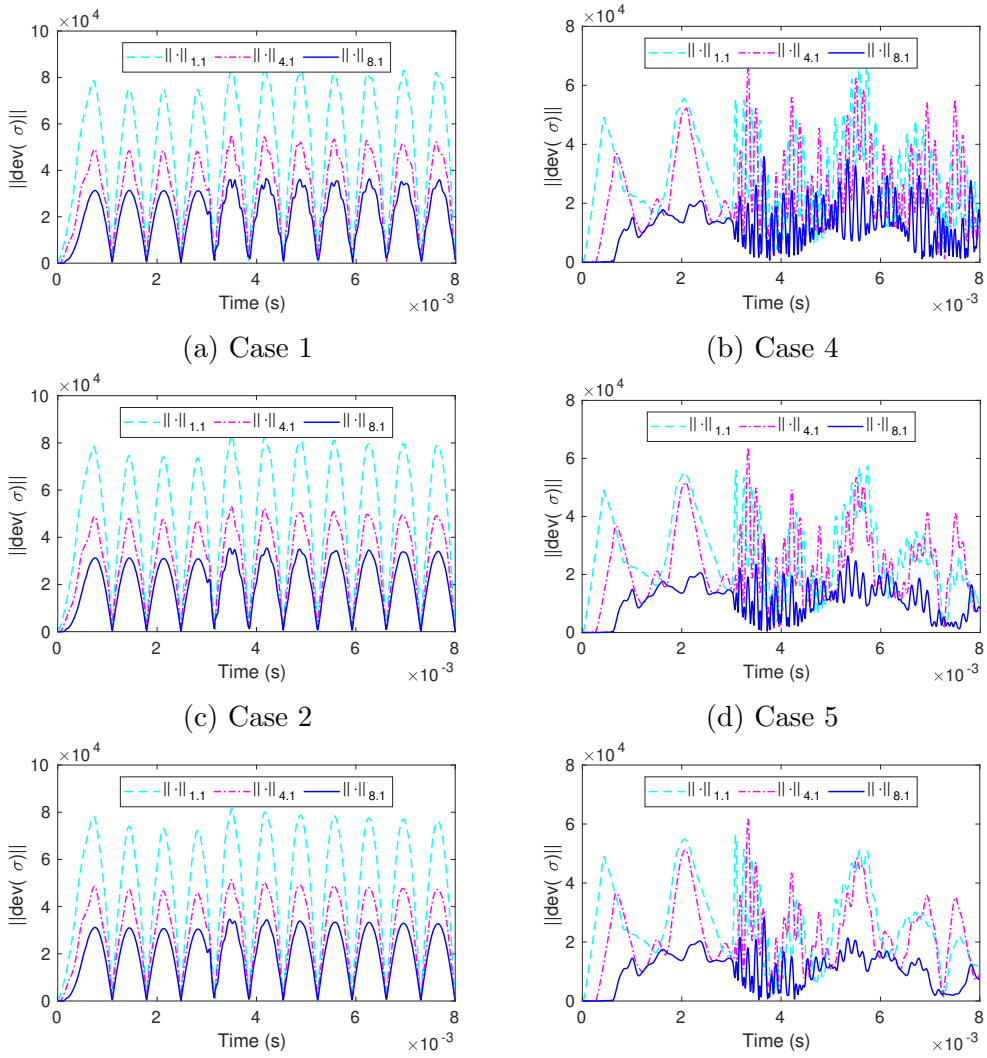

(a) Case 1 (b) Case 4

(c) Case 2 (d) Case 5

(e) Case 3 (f) Case 6

Fig. 15: Stress under visco-plastic regime (ED scheme)

The stiff model is discretized via 16 elements as in Figs. 16a,c and via 32 elements as in Figs. 16b,d, respectively. The energy-decaying scheme results obtained with dissipation factors $(\alpha, \beta) \in \{(0.01, 0.01), (0.1, 0.1)\}$ are then evaluated with the two above discrete models, where only elastic regime is considered. In Figs. 16a,c, the higher values of α and β are chosen, the faster higher frequency modes are filtered out for the stiff system with coarse mesh. In contrast, the lower values of α and β are chosen, the slower higher frequency modes are filtered out from the system with fine mesh, as in Figs. 16b,d. Moreover, any finer mesh can better resolve high frequencies, and thus produces smaller numerical dissipation and less significant on amplitude decay due to higher-frequency modes. From the above observations, the most proper choice for the numerical dissipation factors α and β depends both on the type of system (soft vs. stiff), and on the element size in the mesh. This best choice would be left to the users depending upon the kind of results that are the most acceptable for them. Practically, it is recommended that the higher values of dissipation factors (α, β) should be chosen for a system with coarser mesh than those for a system with finer mesh.

The visco-plastic problem itself dissipates energy through the visco-plastic strain. The energy decaying scheme can be employed if the user expects that the external forces can lead to a significant high frequency modes, in which the contribution from these modes should be dissipated especially on a coarse mesh where they cannot be properly resolved. Meanwhile, the energy conserving scheme can be selected within any case, regardless of elastic or visco-plastic

regimes. It is recorded that the dynamic problem coupled with visco-plastic regime is solved within 3 iterations under quadratic convergence rate (energy residual up-to 10^{-15}).

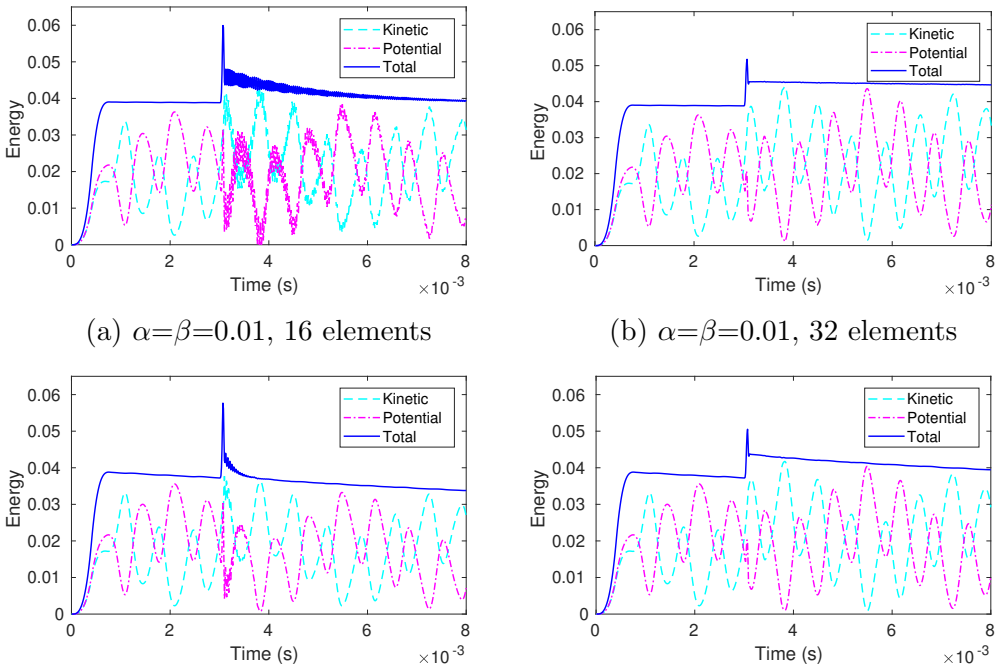

(a) α=β=0.01, 16 elements (b) α=β=0.01, 32 elements

(c) α=β=0.1, 16 elements (d) α=β=0.1, 32 elements

Fig. 16: Stress under elastic regime (stiff model-ED scheme)

5 Conclusions and Discussions

The solution method for visco-plasticity problem proposed herein validates the choice of the Hellinger-Reissner variational principle and the hybrid-stress finite element approximation to deliver a superior accuracy of stress field. Namely, by considering both displacement and stress fields as independent variables does increase the problem size with respect to conventional displacement-based finite element approach, but it also provides the possibility for using coarse mesh with high stress accuracy and a very efficient solution employing consistent tangent elasto-viscoplastic modulus.

The main thrust in this work is further directed to dynamics problem by developing the energy conserving (EC) and the energy decaying (ED) schemes. Both of these schemes are capable of controlling stability of numerical computations. The proposed algorithm shows very satisfying results for a number of numerical simulations, where the computation's stability is enforced by preserving the total energy in elastic regime under EC scheme, or by eventual numerical dissipation that is proved capable of decaying of high frequencies modes which cannot be resolved properly on a coarse finite element mesh under ED scheme. The dissipation parameters α and β in ED scheme can be chosen with respect to mesh size. Practically, the higher values of α and β yield faster dissipation of inappropriate high-frequency modes for a system with coarse mesh. By contrast, these parameters can be selected relatively lower for a system with fine mesh which has fewer unresolved high frequencies and thus automatically reduce the numerical dissipation.

Thanks to the fast convergence and stability of the time-stepping scheme, the proposed formulation can have a potential for other non-linear dynamic problems. In particular, the hybrid-stress interpolation can provide not only an enhanced accuracy of stress field, but also the desirable smoothness of stress approximation, which is of special interest for capturing the wave propagation phenomena.

Acknowlegdement

This work is financially supported under the research project SELT-TUM by Agence Nationale de la Recherche (ANR). Moreover, Prof. Adnan Ibrahimbegovic is also supported by Institut Universitaire de France (IUF). These sources of funding are gratefully acknowledged.

References

[Armero, 2006] Armero, F. (2006). Energy-dissipative momentum-conserving time-stepping algorithms for finite strain multiplicative plasticity. *Computer Methods in Applied Mechanics and Engineering*, 195(37-40):4862–4889.

[Artioli et al., 2007] Artioli, E., Auricchio, F., and da Veiga, L. B. (2007). Second-order accurate integration algorithms for von-mises plasticity with a nonlinear kinematic hardening mechanism. *Computer Methods in Applied Mechanics and Engineering*, 196(9-12):1827–1846.

[Auricchio et al., 2013] Auricchio, F., Balduzzi, G., and Lovadina, C. (2013). The dimensional reduction modelling approach for 3d beams: Differential equations and finite-element solutions based on hellinger–reissner principle. *International Journal of Solids and Structures*, 50(25-26):4184–4196.

[Auricchio et al., 2015] Auricchio, F., Balduzzi, G., and Lovadina, C. (2015). The dimensional reduction approach for 2d non-prismatic beam modelling: a solution based on hellinger–reissner principle. *International Journal of Solids and Structures*, 63:264–276.

[Bathe and Baig, 2005] Bathe, K.-J. and Baig, M. M. I. (2005). On a composite implicit time integration procedure for nonlinear dynamics. *Computers & Structures*, 83(31-32):2513–2524.

[Chorin et al., 1978] Chorin, A. J., Hughes, T. J. R., McCracken, M. F., and Marsden, J. E. (1978). Product formulas and numerical algorithms. *Communications on Pure and Applied Mathematics*, 31(2):205–256.

[Erlicher et al., 2002] Erlicher, S., Bonaventura, L., and Bursi, O. S. (2002). The analysis of the generalized-α method for non-linear dynamic problems. *Computational Mechanics*, 28(2):83–104.

[Hilber et al., 1977] Hilber, H. M., Hughes, T. J. R., and Taylor, R. L. (1977). Improved numerical dissipation for time integration algorithms in structural dynamics. *Earthquake Engineering & Structural Dynamics*, 5(3):283–292.

[Hughes and Taylor, 1978] Hughes, T. J. R. and Taylor, R. L. (1978). Unconditionally stable algorithms for quasi-static elasto/visco-plastic finite element analysis. *Computers & Structures*, 8(2):169–173.

[Ibrahimbegovic, 2009] Ibrahimbegovic, A. (2009). *Nonlinear solid mechanics: theoretical formulations and finite element solution methods*, volume 160. Springer Science & Business Media.

[Ibrahimbegovic et al., 1998] Ibrahimbegovic, A., Gharzeddine, F., and Chorfi, L. (1998). Classical plasticity and viscoplasticity models reformulated: theoretical basis and numerical implementation. *International journal for numerical methods in engineering*, 42(8):1499–1535.

[Ibrahimbegovic and Mamouri, 2002] Ibrahimbegovic, A. and Mamouri, S. (2002). Energy conserving/decaying implicit time-stepping scheme for nonlinear dynamics of three-dimensional beams undergoing finite rotations. *Computer Methods in Applied Mechanics and Engineering*, 191(37-38):4241–4258.

[Lubliner, 2008] Lubliner, J. (2008). *Plasticity theory*. Courier Corporation.

[Mahnken et al., 2013] Mahnken, R., Wolff, M., and Cheng, C. (2013). A multi-mechanism model for cutting simulations combining visco-plastic asymmetry and phase transformation. *International Journal of Solids and Structures*, 50(20-21):3045–3066.

[Neto et al., 1996] Neto, E. D. S., Peric, D., Dutko, M., and Owen, D. (1996). Design of simple low order finite elements for large strain analysis of nearly incompressible solids. *International Journal of Solids and Structures*, 33(20-22):3277–3296.

[Neto et al., 2005] Neto, E. D. S., Pires, F. A., and Owen, D. (2005). F-bar-based linear triangles and tetrahedra for finite strain analysis of nearly incompressible solids. part i: formulation and benchmarking. *International Journal for Numerical Methods in Engineering*, 62(3):353–383.

[Pian and Sumihara, 1984] Pian, T. H. H. and Sumihara, K. (1984). Rational approach for assumed stress finite elements. *International Journal for Numerical Methods in Engineering*, 20(9):1685–1695.

[Pipard et al., 2013] Pipard, J. M., Balan, T., Farid, A. M., and Xavier, L. (2013). Elasto-visco-plastic modeling of mild steels for sheet forming applications over a large range of strain rates. *International Journal of Solids and Structures*, 50(16-17):2691–2700.

[Taylor, 2014] Taylor, R. L. (2014). Feap–finite element analysis program published: 2014. *Publisher: University of California, Berkeley, URL: http://www.ce.berkeley/feap*.

[Viebahn et al., 2018] Viebahn, N., Steeger, K., and Schröder, J. (2018). A simple and efficient hellinger–reissner type mixed finite element for nearly incompressible elasticity. *Computer Methods in Applied Mechanics and Engineering*, 340:278–295.

[Wilson and Ibrahimbegovic, 1990] Wilson, E. L. and Ibrahimbegovic, A. (1990). Use of incompatible displacement modes for the calculation of element stiffnesses or stresses. *Finite Elements in Analysis and Design*, 7(3):229–241.

[Zienkiewicz and Cormeau, 1974] Zienkiewicz, O. C. and Cormeau, I. C. (1974). Visco-plasticity and plasticity an alternative for finite element solution of material nonlinearities. In *Computing Methods in Applied Sciences and Engineering Part 1*, pages 259–287. Springer.

[Zienkiewicz et al., 2005] Zienkiewicz, O. C., Taylor, R. L., and Zhu, J. Z. (2005). *The finite element method: its basis and fundamentals*. Elsevier.